System Equivalent Model Mixing: A Modal Domain Formulation

Miha Pogačar[a], Domen Ocepek[a], Francesco Trainotti[b], Gregor Čepon[a,*], Miha Boltežar[a]

[a] *University of Ljubljana, Faculty of Mechanical Engineering, Aškerčeva cesta 6, 1000 Ljubljana, Slovenia*
[b] *Technical University of Munich, Faculty of Mechanical Engineering, Chair of Applied Mechanics, Boltzmannstr. 15, 85748 Garching, Germany*

Publication:
Pogačar, M., Ocepek, D., Trainotti F., Čepon, G. and Boltežar, M. (2022). System equivalent model mixing: A modal domain formulation. Mechanical Systems and Signal Processing, 177, 109239 (https://doi.org/10.1016/j.ymssp.2022.109239).

Abstract

Hybrid modeling is an increasingly common procedure for predicting the structural dynamics of complex products. System equivalent model mixing (SEMM), a dynamic substructuring-based method, is a recent addition to the field. Its implementation within frequency-based substructuring has great potential. Therefore, it is reasonable to explore the options for implementing an equivalent substructuring framework in any of the other substructuring domains. The objective of this paper is to present M-SEMM, system equivalent model mixing in the modal domain. A theoretical derivation reveals that under certain constrained conditions, the proposed methodology is equivalent to the system equivalent reduction expansion process (SEREP), a well-established reduction/expansion technique. When considering the expansion of spatially sparse models with a high modal density, M-SEMM represents a novel expansion method, which can be seen as a potentially useful extension to SEREP. The proposed implementation offers certain advantages, the most notable being a superior ability to disregard spurious modes in the hybrid model. A study of the proposed methodology on a numerical and an experimental case demonstrates its applicability and provides a comparison with SEREP and the original implementation of SEMM in the frequency domain.

Keywords: SEMM, SEREP, model expansion, hybrid modelling, dynamic substructuring

1. Introduction

In the process of designing and developing complex products, a modular approach is increasingly common, with an important aspect being the ability to predict the dynamic properties of the final assembly. This is only possible, however, if we are able to access valid models of the individual components. In a variety of different modeling approaches, we generally distinguish between numerical and experimental methods. Numerical models are typically obtained with a high spatial resolution; however, their accuracy is limited by the available computational power and the ability to realistically model geometry, material properties, boundary conditions, joint properties, etc. On the other hand, experimental models that provide an insight into a real component's dynamics are typically obtained with a lower spatial resolution given the available resources and limitations in physical accessibility. Often, a compromise between different modeling approaches proves to be the best option for the dynamic modeling of the respective component. Therefore, expansion methods can be used to form its hybrid model.

Reduction/expansion methods emerged in the 1960s. They were used to overcome the problem of limited computational power. Guyan static condensation [1] is probably one of the most commonly recognized methods; however, it lacks any consideration of inertial effects. In 1989, originating from a technique to obtain rotational responses from experimental modal data, a technique named the system equivalent reduction expansion process (SEREP) [2] was developed and has since become a popular expansion/reduction method [3–7]. SEREP is

*Corresponding author
Email address: gregor.cepon@fs.uni-lj.si (Gregor Čepon)

defined in the modal domain with one of the possible applications being the expansion of experimental modal data to an unmeasured denser set of degrees of freedom (DOFs), corresponding to an equivalent numerical model.

Recently, a novel expansion methodology named system equivalent model mixing (SEMM) [8] was introduced as a frequency-based substructuring method. This was followed by its comparison with SEREP [9]. Originally, the methodology comprised the basic and the extended formulation. The latter was further augmented in [10] by applying truncated singular-value decomposition (TSVD), thus increasing the method's resilience to experimental errors. SEMM has been successfully employed in a variety of applications, such as dynamic coupling within frequency-based substructuring [8, 11] and substructuring-based joint identification [12, 13]. Although the framework is typically considered for experimental-numerical hybrid modeling, the same procedure can be applied for purely experimental applications, such as improving full-field high-speed [14] or acoustic [15] camera measurements. Another possible application of the expansion method is the detection of inconsistent measurements, which was implemented in similar methodologies using both SEREP [16] and SEMM [17, 18].

Originally, SEMM was introduced as a Lagrange-multiplier frequency-based substructuring (LM-FBS [19]) procedure. Dynamic substructuring, however, differentiates methods for three general representations (spatial, spectral, and state) of dynamic properties. While LM-FBS is rapidly developing within spectral methods, modal substructuring (often also referred to as component-mode synthesis) is firmly established as the earliest spatial subdomain. When considering experimental models, certain differences may occur between the results of frequency-based and modal substructuring. Modelling in the modal domain seems to be more appropriate for substructuring with experimental models of lightly damped structures, for which the modal identification can be performed well [20].

The objective of this paper is to introduce M-SEMM, i.e., system equivalent model mixing in the modal domain. Unlike in the original LM-FBS implementation, due to the modal reduction, we differentiate between a determined and an under-determined type of methodology. A theoretical derivation of the determined type reveals its equivalence to SEREP. The under-determined M-SEMM type, on the other hand, is considered as a novel modal expansion method, whereby like in the original version we distinguish between a basic and an extended formulation.

At first glance, a reformulation of SEMM in the modal domain might be considered as redundant, as it is known that frequency-based methods can also be applied to modal models using modal superposition [20]. However, the implementation "per-mode" instead of "per-frequency-line" leads to differences. Spuriousities often occur in hybrid models, obtained with the basic formulation of frequency-based SEMM. This problem tends to be solved by applying the extended SEMM formulation, which typically smooths out the spurious peaks [8]. Modal implementation, however, makes it possible to completely disregard the spurious dynamics in the hybrid model, while maintaining low computational costs, which could prove beneficial when applied to real-life complex systems.

This paper is organized as follows. The next section summarizes the basic modal substructuring theory, followed by a brief overview of SEREP and SEMM. In Section 4 the proposed M-SEMM methodology is outlined. In Sections 5 and 6 the applicability of the proposed methodology is demonstrated with a numerical and an experimental study, respectively. Finally, the conclusions are drawn in Section 7.

2. Modal substructuring - primal formulation

This section briefly reviews the basic theory of modal substructuring, following the notation in [20]. For substructure s, the linear equations of motion in the physical domain can be written as:

$$\mathbf{M}^{(s)}\,\ddot{\boldsymbol{u}}^{(s)} + \mathbf{C}^{(s)}\,\dot{\boldsymbol{u}}^{(s)} + \mathbf{K}^{(s)}\,\boldsymbol{u}^{(s)} = \boldsymbol{f}^{(s)} + \boldsymbol{g}^{(s)}\,, \tag{1}$$

where $\mathbf{M}^{(s)}$, $\mathbf{C}^{(s)}$ and $\mathbf{K}^{(s)}$ are the corresponding mass, damping, and stiffness matrices. The vector $\boldsymbol{u}^{(s)}$ denotes the substructure's displacements, $\boldsymbol{f}^{(s)}$ is the external force vector, and $\boldsymbol{g}^{(s)}$ is the vector of connecting interface forces. Vectors $\dot{\boldsymbol{u}}^{(s)}$ and $\ddot{\boldsymbol{u}}^{(s)}$ denote the first and second time derivatives of the displacements, respectively.
The dynamics of a substructured system with N components is described by the set of equations[1]:

$$\mathbf{M}\,\ddot{\boldsymbol{u}} + \mathbf{C}\,\dot{\boldsymbol{u}} + \mathbf{K}\,\boldsymbol{u} = \boldsymbol{f} + \boldsymbol{g} \tag{2}$$

$$\mathbf{B}\,\boldsymbol{u} = \mathbf{0} \tag{3}$$

$$\mathbf{L}^{\mathrm{T}}\,\boldsymbol{g} = \mathbf{0}\,, \tag{4}$$

where $\mathbf{M} = \mathrm{diag}\left[\mathbf{M}^{(1)}, \ldots, \mathbf{M}^{(N)}\right]$, $\mathbf{C} = \mathrm{diag}\left[\mathbf{C}^{(1)}, \ldots, \mathbf{C}^{(N)}\right]$, $\mathbf{K} = \mathrm{diag}\left[\mathbf{K}^{(1)}, \ldots, \mathbf{K}^{(N)}\right]$,
and $\boldsymbol{u} = \left\{\boldsymbol{u}^{(1)}, \ldots, \boldsymbol{u}^{(N)}\right\}^{\mathrm{T}}$, $\boldsymbol{f} = \left\{\boldsymbol{f}^{(1)}, \ldots, \boldsymbol{f}^{(N)}\right\}^{\mathrm{T}}$, $\boldsymbol{g} = \left\{\boldsymbol{g}^{(1)}, \ldots, \boldsymbol{g}^{(N)}\right\}^{\mathrm{T}}$.
The constraints between substructures are applied by compatibility and equilibrium conditions in Eqs. (3) and (4).
Within modal substructuring, physical degrees of freedom (DOFs) $\boldsymbol{u}$ are typically reduced to a smaller set of dual generalized DOFs $\boldsymbol{\eta}$:

$$\boldsymbol{u} = \mathbf{R}\,\boldsymbol{\eta}\,, \tag{5}$$

where $\mathbf{R} = \mathrm{diag}\left[\mathbf{R}^{(1)}, \ldots, \mathbf{R}^{(N)}\right]$ is a block-diagonal reduction matrix. By applying the reduction, the system of Eqs. (2)–(4) reformulates to:

$$\mathbf{M}_{\mathrm{m}}\,\ddot{\boldsymbol{\eta}} + \mathbf{C}_{\mathrm{m}}\,\dot{\boldsymbol{\eta}} + \mathbf{K}_{\mathrm{m}}\,\boldsymbol{\eta} = \boldsymbol{f}_{\mathrm{m}} + \boldsymbol{g}_{\mathrm{m}}\,, \tag{6}$$

$$\mathbf{B}_{\mathrm{m}}\,\boldsymbol{\eta} = \mathbf{0}\,, \tag{7}$$

$$\mathbf{L}_{\mathrm{m}}^{\mathrm{T}}\,\boldsymbol{g}_{\mathrm{m}} = \mathbf{0}\,, \tag{8}$$

where $\mathbf{M}_{\mathrm{m}} = \mathbf{R}^{\mathrm{T}}\,\mathbf{M}\,\mathbf{R}$, $\mathbf{C}_{\mathrm{m}} = \mathbf{R}^{\mathrm{T}}\,\mathbf{C}\,\mathbf{R}$, $\mathbf{K}_{\mathrm{m}} = \mathbf{R}^{\mathrm{T}}\,\mathbf{K}\,\mathbf{R}$, $\boldsymbol{f}_{\mathrm{m}} = \mathbf{R}^{\mathrm{T}}\,\boldsymbol{f}$, $\boldsymbol{g}_{\mathrm{m}} = \mathbf{R}^{\mathrm{T}}\,\boldsymbol{g}$,
and $\mathbf{B}_{\mathrm{m}} = \mathbf{B}\,\mathbf{R}$, $\mathbf{L}_{\mathrm{m}} = \mathrm{null}\,(\mathbf{B}_{\mathrm{m}})$.
By introducing the transformation from the dual to the unique set of generalized DOFs $\boldsymbol{\xi}$:

$$\boldsymbol{\eta} = \mathbf{L}_{\mathrm{m}}\,\boldsymbol{\xi}\,, \tag{9}$$

and by pre-multiplication with $\mathbf{L}_{\mathrm{m}}^{\mathrm{T}}$, the system of Eqs. (6)–(8) reduces to the primal formulation of the coupled equation of motion:

$$\tilde{\mathbf{M}}_{\mathrm{m}}\,\ddot{\boldsymbol{\xi}} + \tilde{\mathbf{C}}_{\mathrm{m}}\,\dot{\boldsymbol{\xi}} + \tilde{\mathbf{K}}_{\mathrm{m}}\,\boldsymbol{\xi} = \tilde{\boldsymbol{f}}_{\mathrm{m}}\,, \tag{10}$$

where:
$\tilde{\mathbf{M}}_{\mathrm{m}} = \mathbf{L}_{\mathrm{m}}^{\mathrm{T}}\,\mathbf{M}_{\mathrm{m}}\,\mathbf{L}_{\mathrm{m}}$, $\tilde{\mathbf{C}}_{\mathrm{m}} = \mathbf{L}_{\mathrm{m}}^{\mathrm{T}}\,\mathbf{C}_{\mathrm{m}}\,\mathbf{L}_{\mathrm{m}}$, $\tilde{\mathbf{K}}_{\mathrm{m}} = \mathbf{L}_{\mathrm{m}}^{\mathrm{T}}\,\mathbf{K}_{\mathrm{m}}\,\mathbf{L}_{\mathrm{m}}$, and $\tilde{\mathbf{f}}_{\mathrm{m}} = \mathbf{L}_{\mathrm{m}}^{\mathrm{T}}\,\mathbf{f}_{\mathrm{m}}$.

[1] Note, that if a substructure is to be decoupled from the system, its mass, damping, and stiffness matrices in the global block-diagonal equation of motion are to be assigned as negative.

3. Brief overview of SEREP and SEMM

This section briefly summarizes the established concepts of SEREP and SEMM. For the sake of simplicity, any derivations are omitted, thus only providing final equations for each method. Let us consider two equivalent models, denoted as the parent (par) and the overlay (ov), as depicted in Fig. 1. The naming convention is adopted from the original frequency-based SEMM implementation [8]. The methodologies considered in this paper apply for equivalent models that are either purely numerical, experimental, or combined, provided that they meet the following characteristics:

1. *Parent model*: The inferior dynamic properties of this model are obtained in a dense set of DOFs.
2. *Overlay model*: The superior dynamic properties of this model are obtained in a sparse set of DOFs.

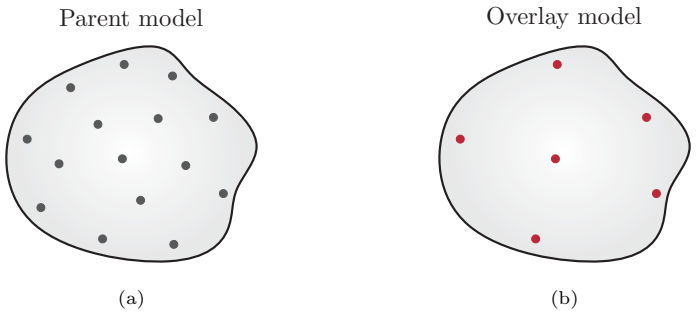

Figure 1: Equivalent models: (a) Parent; (b) Overlay.

The dense set of the parent model's physical DOFs $\boldsymbol{u}^{(\mathrm{par})}$ can be partitioned into the internal (i) and the boundary subset (b) of sizes n_i and n_b, respectively. The internal subset is unique to the dense set of DOFs, whereas the boundary subset is collocated with the sparse subset of the overlay model's DOFs $\boldsymbol{u}^{(\mathrm{ov})}$:

$$\boldsymbol{u}^{(\mathrm{par})} = \begin{bmatrix} \boldsymbol{u}_i^{(\mathrm{par})} \\ \boldsymbol{u}_b^{(\mathrm{par})} \end{bmatrix}, \tag{11}$$

$$\boldsymbol{u}^{(\mathrm{ov})} = \boldsymbol{u}_b^{(\mathrm{ov})}. \tag{12}$$

In some of the following derivations the index g is used to emphasize the combined set of internal and boundary DOFs.

An additional duplicate (sub)-model of the parent model is introduced in the SEMM substructuring process, referred to as the removed model (rem). The resulting hybrid model (hyb) is obtained by expanding the sparse overlay model's dynamics to the dense set of the parent model's DOFs. Similarly, the partitioning of the degrees of freedom also applies for those models:

$$\boldsymbol{u}^{(\mathrm{rem})} = \begin{bmatrix} \boldsymbol{u}_i^{(\mathrm{rem})} \\ \boldsymbol{u}_b^{(\mathrm{rem})} \end{bmatrix}, \tag{13}$$

$$\boldsymbol{u}^{(\mathrm{hyb})} = \begin{bmatrix} \boldsymbol{u}_i^{(\mathrm{hyb})} \\ \boldsymbol{u}_b^{(\mathrm{hyb})} \end{bmatrix}. \tag{14}$$

3.1. SEREP - basic concept

The technique is defined in the modal domain and operates on the modal parameters of the equivalent models. A (truncated) set of mode shapes $\mathbf{\Phi}^{(\mathrm{par})}$ and $\mathbf{\Phi}^{(\mathrm{ov})}$ is considered for the parent and the overlay model, respectively. The parameters $m^{(\mathrm{par})}$ and $m^{(\mathrm{ov})}$ denote the corresponding number of modal vectors. The expanded hybrid model is obtained as[2]:

$$\mathbf{\Phi}^{(\mathrm{hyb})} = \mathbf{\Phi}_g^{(\mathrm{par})} \, \mathbf{\Phi}_b^{(\mathrm{par})\dagger} \, \mathbf{\Phi}_b^{(\mathrm{ov})} \,, \tag{15}$$

where $(\,)^\dagger$ denotes the generalized inverse. The original SEREP methodology [2] clearly distinguishes between a determined and an under-determined type, for which $n_b \geq m^{(\mathrm{par})}$ and $n_b < m^{(\mathrm{par})}$ hold, respectively. The methodology is effective for the determined type, where for $n_b = m^{(\mathrm{par})}$ the hybrid modal vectors represent a solution of the determined problem, and for $n_b > m^{(\mathrm{par})}$, for which the solution of an over-determined problem is obtained in a least-squares sense. The under-determined type, on the other hand, although mathematically applicable, is considered to be of no practical use.

3.2. SEMM - basic concept

The methodology is based on a substructuring framework and consists of a coupling and a decoupling step between the parent, removed and overlay models, as depicted in Fig. 2. Coupling constraints between the removed and overlay models are applied at the sparse set of DOFs. The decoupling constraints between the parent and removed models are applied on either a sparse or a dense set of DOFs, thus differentiating between the basic and the extended SEMM formulation, respectively[3]. The substructuring procedure yields an assembled system, from which the hybrid properties are obtained at the DOFs, corresponding to the parent model.

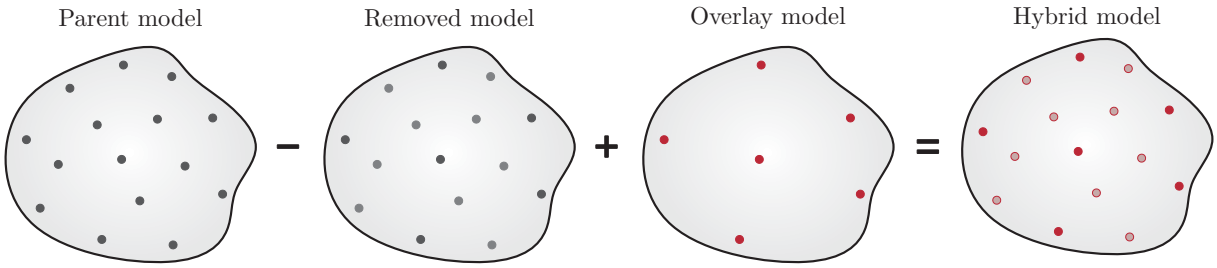

Figure 2: Schematic depiction of SEMM.

The frequency-based SEMM implementation operates on admittance matrices of the equivalent models. Following the DOF partitioning principle defined above, the admittance matrix for the substructure s is given as:

$$\mathbf{Y}^{(s)} = \begin{bmatrix} \mathbf{Y}_{ii}^{(s)} & \mathbf{Y}_{ib}^{(s)} \\ \mathbf{Y}_{bi}^{(s)} & \mathbf{Y}_{bb}^{(s)} \end{bmatrix} .$$

The most efficient implementation of the LM-FBS-based SEMM formulation is given as a single-line equation

[2]Note that since spatial expansion of mode shapes is considered, the general boundary response to be subjected to the expansion process (typically denoted as $\boldsymbol{u}_b$) is replaced by $\mathbf{\Phi}_b^{(\mathrm{ov})}$.

[3]In [8], the extension of the decoupling constraints is considered for an arbitrary subset of internal DOFs. In this paper, however, for simplicity the extended formulation is considered for the full dense set of DOFs.

for the basic and the extended formulation, respectively:

$$\mathbf{Y}^{(\mathrm{hyb})} = \mathbf{Y}_{gg}^{(\mathrm{par})} - \mathbf{Y}_{gb}^{(\mathrm{par})}\,\mathbf{Y}_{bb}^{(\mathrm{rem})\,-1}\left(\mathbf{Y}_{bb}^{(\mathrm{rem})} - \mathbf{Y}_{bb}^{(\mathrm{ov})}\right)\mathbf{Y}_{bb}^{(\mathrm{rem})\,-1}\,\mathbf{Y}_{bg}^{(\mathrm{par})}\,, \tag{16}$$

$$\mathbf{Y}^{(\mathrm{hyb})} = \mathbf{Y}_{gg}^{(\mathrm{par})} - \mathbf{Y}_{gg}^{(\mathrm{par})}\,\mathbf{Y}_{bg}^{(\mathrm{rem})\,\dagger}\left(\mathbf{Y}_{bb}^{(\mathrm{rem})} - \mathbf{Y}_{bb}^{(\mathrm{ov})}\right)\mathbf{Y}_{gb}^{(\mathrm{rem})\,\dagger}\,\mathbf{Y}_{gg}^{(\mathrm{par})}\,. \tag{17}$$

It is observed that the calculation of the generalized inversion is required in the extended formulation (Eq. (17)), which is typically obtained by performing singular-value decomposition (SVD) and disregarding the zero-valued singular values. A possible extension to this approach is proposed in [10], where an additional truncation of small singular values is performed to improve the method's robustness with regard to experimental errors.

4. M-SEMM - System equivalent model mixing in the modal domain

The derivation of the M-SEMM is based on an equivalent substructuring process, as originally proposed in its frequency-based implementation [8]. For simplicity, we assume proportional damping for all the substructures (within the SEMM framework these are the parent, removed and overlay equivalent models).

4.1. Modal transformation and un-coupled equation of motion

A set of $m^{(s)}$ mass-normalized free-interface mode shapes $\mathbf{\Phi}^{(s)}$ is considered as a reduction matrix $\mathbf{R}^{(s)}$ for each equivalent model s. Then, the reduction of the physical DOFs $\boldsymbol{u}$ to dual generalized DOFs $\boldsymbol{\eta}$ from Eq. (5) reads as:

$$\begin{bmatrix} \boldsymbol{u}_i^{(\mathrm{par})} \\ \boldsymbol{u}_b^{(\mathrm{par})} \\ \boldsymbol{u}_i^{(\mathrm{rem})} \\ \boldsymbol{u}_b^{(\mathrm{rem})} \\ \boldsymbol{u}_b^{(\mathrm{ov})} \end{bmatrix} = \begin{bmatrix} \mathbf{\Phi}_i^{(\mathrm{par})} & \mathbf{0} & \mathbf{0} \\ \mathbf{\Phi}_b^{(\mathrm{par})} & \mathbf{0} & \mathbf{0} \\ \mathbf{0} & \mathbf{\Phi}_i^{(\mathrm{rem})} & \mathbf{0} \\ \mathbf{0} & \mathbf{\Phi}_b^{(\mathrm{rem})} & \mathbf{0} \\ \mathbf{0} & \mathbf{0} & \mathbf{\Phi}_b^{(\mathrm{ov})} \end{bmatrix} \begin{bmatrix} \boldsymbol{\eta}^{(\mathrm{par})} \\ \boldsymbol{\eta}^{(\mathrm{rem})} \\ \boldsymbol{\eta}^{(\mathrm{ov})} \end{bmatrix}, \tag{18}$$

and the un-coupled equation of motion Eq. (6) simplifies to:

$$\begin{bmatrix} \mathbf{I}^{(\mathrm{par})} & \mathbf{0} & \mathbf{0} \\ \mathbf{0} & -\mathbf{I}^{(\mathrm{rem})} & \mathbf{0} \\ \mathbf{0} & \mathbf{0} & \mathbf{I}^{(\mathrm{ov})} \end{bmatrix} \begin{bmatrix} \ddot{\boldsymbol{\eta}}^{(\mathrm{par})} \\ \ddot{\boldsymbol{\eta}}^{(\mathrm{rem})} \\ \ddot{\boldsymbol{\eta}}^{(\mathrm{ov})} \end{bmatrix} + \begin{bmatrix} 2\,\boldsymbol{\zeta}_r^{(\mathrm{par})}\,\boldsymbol{\omega}_r^{(\mathrm{par})} & \mathbf{0} & \mathbf{0} \\ \mathbf{0} & -2\,\boldsymbol{\zeta}_r^{(\mathrm{rem})}\,\boldsymbol{\omega}_r^{(\mathrm{rem})} & \mathbf{0} \\ \mathbf{0} & \mathbf{0} & 2\,\boldsymbol{\zeta}_r^{(\mathrm{ov})}\,\boldsymbol{\omega}_r^{(\mathrm{ov})} \end{bmatrix} \begin{bmatrix} \dot{\boldsymbol{\eta}}^{(\mathrm{par})} \\ \dot{\boldsymbol{\eta}}^{(\mathrm{rem})} \\ \dot{\boldsymbol{\eta}}^{(\mathrm{ov})} \end{bmatrix} + \\ \begin{bmatrix} \boldsymbol{\omega}_r^{2\,(\mathrm{par})} & \mathbf{0} & \mathbf{0} \\ \mathbf{0} & -\boldsymbol{\omega}_r^{2\,(\mathrm{rem})} & \mathbf{0} \\ \mathbf{0} & \mathbf{0} & \boldsymbol{\omega}_r^{2\,(\mathrm{ov})} \end{bmatrix} \begin{bmatrix} \boldsymbol{\eta}^{(\mathrm{par})} \\ \boldsymbol{\eta}^{(\mathrm{rem})} \\ \boldsymbol{\eta}^{(\mathrm{ov})} \end{bmatrix} = \begin{bmatrix} \boldsymbol{f}_{\mathrm{m}}^{(\mathrm{par})} \\ \boldsymbol{f}_{\mathrm{m}}^{(\mathrm{rem})} \\ \boldsymbol{f}_{\mathrm{m}}^{(\mathrm{ov})} \end{bmatrix} + \begin{bmatrix} \boldsymbol{g}_{\mathrm{m}}^{(\mathrm{par})} \\ \boldsymbol{g}_{\mathrm{m}}^{(\mathrm{rem})} \\ \boldsymbol{g}_{\mathrm{m}}^{(\mathrm{ov})} \end{bmatrix}. \tag{19}$$

For a substructure s, $\mathbf{I}^{(s)}$ is an identity matrix, and $\boldsymbol{\omega}_r^{2\,(s)}$ and $\boldsymbol{\zeta}_r^{(s)}$ are the diagonal matrices of the substructure's eigenvalues and damping ratios, respectively[4].

4.2. Different types of compatibility conditions

4.2.1. Coupling step

In the coupling step, compatibility is enforced between the removed and the overlay model at the boundary DOFs. In terms of physical coordinates, the compatibility condition is given as:

$$\boldsymbol{u}_b^{(\mathrm{rem})} = \boldsymbol{u}_b^{(\mathrm{ov})}\,. \tag{20}$$

[4]The negative sign for the removed model's dynamics in the equation of motion corresponds to the decoupling process.

Considering the transformation to the modal domain (Eq. (18)), the physical compatibility in terms of generalized coordinates is transformed into:

$$\boldsymbol{\Phi}_b^{(\mathrm{rem})}\,\boldsymbol{\eta}^{(\mathrm{rem})} = \boldsymbol{\Phi}_b^{(\mathrm{ov})}\,\boldsymbol{\eta}^{(\mathrm{ov})}\,, \tag{21}$$

where $\boldsymbol{\Phi}_b^{(\mathrm{rem})} \in \mathbb{R}^{n_b \times m^{(\mathrm{rem})}}$ and $\boldsymbol{\Phi}_b^{(\mathrm{ov})} \in \mathbb{R}^{n_b \times m^{(\mathrm{ov})}}$, thus applying n_b constraints.

The expansion process in M-SEMM operates on $m^{(\mathrm{ov})}$ overlay model's mode shapes. In this way the same number of hybrid modes is expected as the output of the method. In the coupling step, constraints are applied between the removed and overlay models, with the total number of dual generalized coordinates equal to $m^{(\mathrm{rem})} + m^{(\mathrm{ov})}$. Therefore, in order to retain no less than the expected number of unique generalized DOFs, it is generally not viable to apply more than $m^{(\mathrm{rem})}$ constraints. Otherwise, due to additional constraints, the hybrid model would contain fewer modes than the original overlay model.

Although theoretically applicable, such cases are avoided within the paper. Instead, a weak form of constraints is considered when $n_b > m^{(\mathrm{rem})}$ holds. In the modal domain, it is natural to adopt the concept of modal constraints, originally presented within the transmission simulator method [21]. Modal compatibility is acquired by pre-multiplying the Eq. (21) by either $\boldsymbol{\Phi}_b^{(\mathrm{rem})\dagger}$ or $\boldsymbol{\Phi}_b^{(\mathrm{ov})\dagger}$, thus satisfying the physical compatibility in a least-squares sense.

In a typical SEMM application the overlay model is often obtained experimentally, while the removed model is usually numerical. As we tend to avoid the inversion of experimental data and thus the enhancement of experimental errors, in the following the modal vectors of the removed model are considered for the inversion[5]:

$$\mathbf{I}^{(\mathrm{rem})}\,\boldsymbol{\eta}^{(\mathrm{rem})} = \boldsymbol{\Phi}_b^{(\mathrm{rem})\dagger}\,\boldsymbol{\Phi}_b^{(\mathrm{ov})}\,\boldsymbol{\eta}^{(\mathrm{ov})}\,, \tag{22}$$

where $\mathbf{I}^{(\mathrm{rem})}$ is the $m^{(\mathrm{rem})} \times m^{(\mathrm{rem})}$ identity matrix and $\boldsymbol{\Phi}_b^{(\mathrm{rem})\dagger}\,\boldsymbol{\Phi}_b^{(\mathrm{ov})} \in \mathbb{R}^{m^{(\mathrm{rem})} \times m^{(\mathrm{ov})}}$. Hence, the number of coupling constraints is reduced to $m^{(\mathrm{rem})}$.

4.2.2. Decoupling step - basic formulation

The decoupling compatibility in the basic SEMM formulation is applied between the parent and the removed models at the boundary DOFs:

$$\boldsymbol{u}_b^{(\mathrm{par})} = \boldsymbol{u}_b^{(\mathrm{rem})}\,. \tag{23}$$

In terms of generalized coordinates, the physical compatibility reads as:

$$\boldsymbol{\Phi}_b^{(\mathrm{par})}\,\boldsymbol{\eta}^{(\mathrm{par})} = \boldsymbol{\Phi}_b^{(\mathrm{rem})}\,\boldsymbol{\eta}^{(\mathrm{rem})}\,. \tag{24}$$

Given that the removed model is a duplicate sub-model of the parent model, the following relations hold: $\boldsymbol{\Phi}_b^{(\mathrm{par})} = \boldsymbol{\Phi}_b^{(\mathrm{rem})} \in \mathbb{R}^{n_b \times m^{(\mathrm{rem})}}$ and $m^{(\mathrm{par})} = m^{(\mathrm{rem})}$. The corresponding decoupling compatibility condition consists of n_b constraints. Like in the coupling step, modal weakening is considered when $n_b > m^{(\mathrm{rem})}$. By pre-multiplying Eq. (24) with $\boldsymbol{\Phi}_b^{(\mathrm{par})\dagger}$ or $\boldsymbol{\Phi}_b^{(\mathrm{rem})\dagger}$, the modal compatibility reads as:

$$\mathbf{I}^{(\mathrm{par})}\,\boldsymbol{\eta}^{(\mathrm{par})} = \mathbf{I}^{(\mathrm{rem})}\,\boldsymbol{\eta}^{(\mathrm{rem})}\,, \tag{25}$$

with $\mathbf{I}^{(\mathrm{par})}$ and $\mathbf{I}^{(\mathrm{rem})}$ being identity matrices, thus reducing the number of constraints to $m^{(\mathrm{rem})}$.

[5]However, in the case of an atypical application, there might be a need to revisit this step and adjust the formulation by selecting a different projection basis.

4.2.3. Decoupling step - extended formulation

Availability of the full parent and removed model allows for an extension of the decoupling interface. Such an extension has already been proposed in the original frequency-based SEMM framework [8] to smooth-out the spuriousities by improving the observability and controllability of the decoupling interface. The extended compatibility condition between the parent and removed models is given as:

$$\boldsymbol{u}_g^{(\mathrm{par})} = \boldsymbol{u}_g^{(\mathrm{rem})} \,. \tag{26}$$

However, due to the duplicity of the parent and removed model, such an interface extension results in a physically indeterminate problem. To explain the origin of spuriousities and indeterminacy, an elementary example of the SEMM process is presented in Fig. 3. For simplicity, the example is presented in the physical domain, however, the concepts apply generally. Let us consider equivalent models of a 2 DOF system. The dynamics of the overlay model are only obtained in the boundary DOF, thus its internal DOF is depicted as transparent. Note that ideally, the expected outcome of the expansion process would provide a full 2-DOF overlay model.

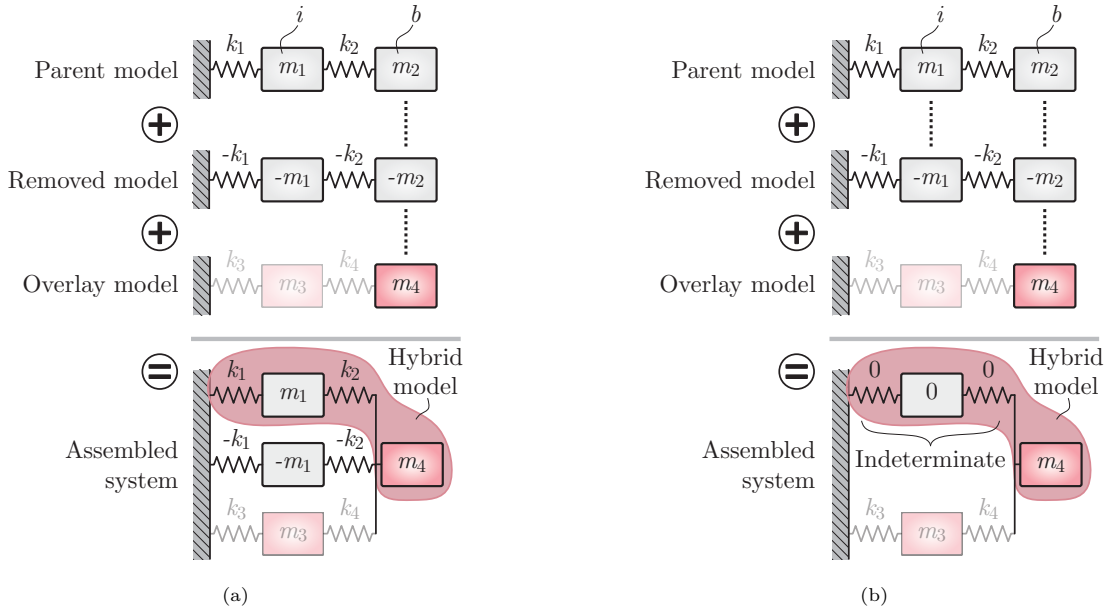

Figure 3: SEMM - elementary example: (a) Basic decoupling compatibility; (b) Indeterminacy of the extended decoupling compatibility.

From the depiction in Fig. 3a however, it is evident that the assembled system, obtained by the basic SEMM substructuring procedure, has 4 DOFs. Even though the hybrid model is obtained at the two parent-related DOFs, the corresponding dynamics generally exhibit the 4-DOF nature of the assembled system. This explains the origin of spurious modes in the hybrid model.

To improve the decoupling process and therefore reduce the occurrence of spurious modes, the decoupling interface between the parent and removed models can be extended to the full set of DOFs, as depicted in Fig. 3b. However, the decoupling of two duplicate models at the internal DOFs yields an indeterminate dynamic system, which is for the given case evident from obtaining a DOF with zero mass and stiffness.

In the original frequency-based SEMM, the indeterminacy is mathematically reflected as a singularity of the interface flexibility matrix, which results in the inapplicability of its direct inversion. The problem is overcome by applying a generalized inverse, which can also be interpreted as an implicit weakening of the decoupling

constraints[6]. The corresponding weakened decoupling compatibility can be written as:

$$\mathbf{Y}_{gb}^{(\mathrm{rem})\dagger}\,\boldsymbol{u}_g^{(\mathrm{par})} = \mathbf{Y}_{gb}^{(\mathrm{rem})\dagger}\,\boldsymbol{u}_g^{(\mathrm{rem})}\,, \tag{27}$$

where $\mathbf{Y}_{gb}^{(\mathrm{rem})\dagger} \in \mathbb{R}^{n_b \times n_g}$ is the generalized inverse of an admittance sub-matrix of the removed model, thus applying n_b constraints[7]. Although the number of constraint equations is the same as in the basic formulation, an extended compatibility condition takes into account the dynamics of the full (boundary and internal) set of DOFs in a frequency-dependent manner. This typically improves the efficiency of the decoupling process, hence the ability of the extended SEMM formulation to smooth-out the spuriousities that are otherwise often present in hybrid models, obtained using the basic formulation.

Considering the proportional viscous damping model and denoting ${}_r\boldsymbol{\phi}^{(\mathrm{s})}$ as the r-th eigenvector in $\boldsymbol{\Phi}^{(\mathrm{s})}$ and ω as the angular frequency, the admittance matrix $\mathbf{Y}_{gb}^{(\mathrm{rem})}$ can be obtained with the following modal superposition:

$$\mathbf{Y}_{gb}^{(\mathrm{rem})}(\omega) = \sum_{r=1}^{m^{(\mathrm{rem})}} \frac{{}_r\boldsymbol{\phi}_g^{(\mathrm{rem})}\,{}_r\boldsymbol{\phi}_b^{(\mathrm{rem})\mathrm{T}}}{\omega_r^{(\mathrm{rem})2} - \omega^2 + 2\,\mathrm{j}\,\omega\,\zeta_r^{(\mathrm{rem})}\,\omega_r^{(\mathrm{rem})}}\,. \tag{28}$$

Given that admittance is a priori a function of frequency, its pseudo-inversion per frequency line results in frequency-dependent weakening of the compatibility condition. To adopt this approach and modify it for use in the modal domain, we propose a "mode-dependent" weakening approach.

For the evaluation of the k-th hybrid mode, the weakening basis is obtained as an un-damped[8] parent model's admittance (28) at the frequency $\omega = \omega_k^{(\mathrm{hyb})}$. Such an approach is not applicable in most substructuring applications as the eigenfrequencies of the assembled system are generally not known. However, M-SEMM yields an exception since the overlay model's eigenfrequencies are always present in the hybrid solution, as will become apparent from further derivations. Therefore, assuming $\omega = \omega_k^{(\mathrm{hyb})} = \omega_k^{(\mathrm{ov})}$, the weakening basis used in the expansion process of the k-th hybrid mode is given as:

$$\mathbf{W}_k = \sum_{r=1}^{m^{(\mathrm{rem})}} \frac{{}_r\boldsymbol{\phi}_g^{(\mathrm{rem})}\,{}_r\boldsymbol{\phi}_b^{(\mathrm{rem})\mathrm{T}}}{\omega_r^{(\mathrm{rem})2} - \omega_k^{(\mathrm{ov})2}}\,; \quad k = 1, \dots m^{(\mathrm{ov})}\,. \tag{29}$$

The proposed weakening basis can be interpreted as a weighted superposition of the parent model's modal constant matrices, for which the weights depend of the deviation between the r-th removed model's and k-th overlay's eigenvalue. Let us consider in this way a special case when $\omega_r^{(\mathrm{rem})2} = \omega_k^{(\mathrm{ov})2}$, for which Eq. (29) appears indeterminate. Then, the r-th term in the series infinitely prevails over all the others and can therefore be considered as the sole contribution in the generation of the projection basis. For a single term, any weighting is irrelevant, thus it is reasonable to disregard the indefinite denominator. The weakening basis is then represented by the r-th matrix of the modal constants ${}_r\boldsymbol{\phi}_g^{(\mathrm{rem})}\,{}_r\boldsymbol{\phi}_b^{(\mathrm{rem})\mathrm{T}}$, for which columns are linearly dependent. Accordingly, a single effective constraint equation is applied and the corresponding weakening basis is simplified to $\mathbf{W}_k = {}_r\boldsymbol{\phi}_g^{(\mathrm{rem})}$.

By pre-multiplying Eq. (26) and considering the modal transformation (Eq. (18)), the proposed approximation of Eq. (27) (at k-th natural frequency) for the use in the modal domain reads as:

$$\mathbf{W}_k^{\dagger}\,\boldsymbol{\Phi}_g^{(\mathrm{par})}\,\boldsymbol{\eta}^{(\mathrm{par})} = \mathbf{W}_k^{\dagger}\,\boldsymbol{\Phi}_g^{(\mathrm{rem})}\,\boldsymbol{\eta}^{(\mathrm{rem})}\,. \tag{30}$$

[6]For the mathematical derivation, an interested reader is referred to the appendix.

[7]If $\mathbf{Y}_{gb}^{(\mathrm{rem})}$ is singular at a frequency line, then the number of effective constraints is further reduced to the rank $\left(\mathbf{Y}_{gb}^{(\mathrm{rem})}\right)$

[8]Damping is omitted for simplicity, to retain the real-valued system matrices of the hybrid model.

Note that the weakening basis needs to be re-evaluated for each (k-th) hybrid mode, while the resulting number of constraints is equal to $\mathrm{rank}(\mathbf{W}_k) \leq n_b$. If $\mathbf{W}_k$ is almost singular, similarly as in the frequency-based implementation [10], the conditioning of the projection space can be improved by applying truncated singular-value decomposition (TSVD). Disregarding the small singular values results in an additional weakening, thus further reducing the number of decoupling constraints.

When the number of applied constraints is greater than $m^{(\mathrm{rem})}$, the modal compatibility is obtained by pre-multiplying Eq. (30) by $\left(\mathbf{W}_k^\dagger \, \mathbf{\Phi}_g^{(\mathrm{rem})}\right)^\dagger$ or $\left(\mathbf{W}_k^\dagger \, \mathbf{\Phi}_g^{(\mathrm{par})}\right)^\dagger$, which results in the equivalent to Eq. (22).

4.3. Deriving M-SEMM

Any of the discussed coupling and decoupling compatibility formulations from the previous section can generally be written in the form:

$$\mathbf{P}_1 \, \boldsymbol{\eta}^{(\mathrm{rem})} \quad - \quad \mathbf{P}_2 \, \boldsymbol{\eta}^{(\mathrm{ov})} = \mathbf{0} \,, \tag{31}$$

$$\mathbf{P}_3 \, \boldsymbol{\eta}^{(\mathrm{par})} \quad - \quad \mathbf{P}_3 \, \boldsymbol{\eta}^{(\mathrm{rem})} = \mathbf{0} \,, \tag{32}$$

which, by adopting the matrix form of the compatibility condition form Eq. (7), reads as:

$$\underbrace{\begin{bmatrix} \mathbf{0} & \mathbf{P}_1 & -\mathbf{P}_2 \\ \mathbf{P}_3 & -\mathbf{P}_3 & \mathbf{0} \end{bmatrix}}_{\mathbf{B}_\mathrm{m}} \begin{bmatrix} \boldsymbol{\eta}^{(\mathrm{par})} \\ \boldsymbol{\eta}^{(\mathrm{rem})} \\ \boldsymbol{\eta}^{(\mathrm{ov})} \end{bmatrix} = \mathbf{0} \,. \tag{33}$$

Following Eq. (9), the primal substructuring operator $\mathbf{L}_\mathrm{m} = \mathrm{null}(\mathbf{B}_\mathrm{m})$ enables the transformation:

$$\begin{bmatrix} \boldsymbol{\eta}^{(\mathrm{par})} \\ \boldsymbol{\eta}^{(\mathrm{rem})} \\ \boldsymbol{\eta}^{(\mathrm{ov})} \end{bmatrix} = \underbrace{\begin{bmatrix} \mathbf{L}_\mathrm{m}^{(\mathrm{par})} \\ \mathbf{L}_\mathrm{m}^{(\mathrm{rem})} \\ \mathbf{L}_\mathrm{m}^{(\mathrm{ov})} \end{bmatrix}}_{\mathbf{L}_\mathrm{m}} \boldsymbol{\xi}^{(\mathrm{hyb})} \,, \tag{34}$$

where the number of unique generalized DOFs $\boldsymbol{\xi}^{(\mathrm{hyb})}$ is equal to $\mathrm{rank}\,(\mathbf{L}_\mathrm{m})$.

At this point let us introduce the classification to an over-determined, determined and under-determined M-SEMM type. The over-determined type corresponds to the over-constrained case, for which the resulting number of unique generalized DOFs is lower than $m^{(\mathrm{ov})}$. In this paper, such a case is only considered if it is beforehand transformed into the determined type by applying the modal constraints. For the determined type, the number of unique, generalized DOFs equals exactly $m^{(\mathrm{ov})}$, while the under-determined type corresponds to an under-constrained case, for which an excessive number of unique, generalized DOFs is obtained in the hybrid model.

Assuming that n_b constraints[9] are applied in the coupling and the decoupling step, this translates to the conditions $n_b > m^{(\mathrm{par})}$, $n_b = m^{(\mathrm{par})}$ and $n_b < m^{(\mathrm{par})}$ for the over-determined, determined and under-determined cases, respectively. The corresponding shapes of the $\mathbf{B}_\mathrm{m}$ matrices are depicted in Fig. 4.

In the following, a determined type and an under-determined M-SEMM type are discussed in detail.

[9]For simplicity, the possibility of additional weakening by applying TSVD is disregarded in the general classification of types. In the following, such procedures are only considered within the analysis of the under-determined type.

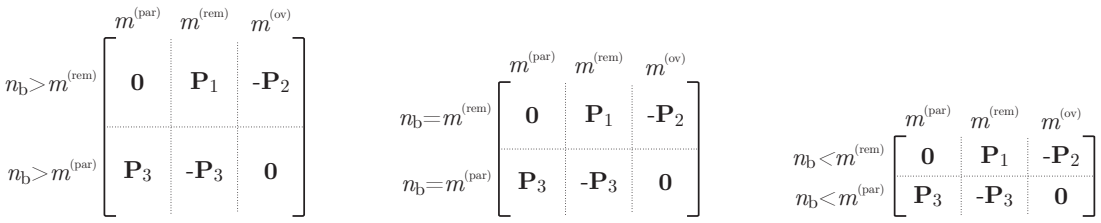

Figure 4: Shape of $\mathbf{B}_\mathrm{m}$ matrix: (a) Over-determined type; (b) Determined type; (c) Under-determined type.

4.3.1. Determined type and its resemblance to SEREP

The determined M-SEMM type is referred to as a case when a hybrid M-SEMM model with exactly $m^{(\mathrm{ov})}$ unique generalized DOFs is obtained by applying $m^{(\mathrm{rem})}$ (independent) constraints for both the coupling and the decoupling step. Among the previously discussed compatibility formulations, this condition holds for the following cases:

1. Basic physical compatibility (Eqs. (21) and (24)) and $n_b = m^{(\mathrm{rem})}$:
   $\mathbf{P}_1 = \mathbf{P}_3 = \mathbf{\Phi}_b^{(\mathrm{rem})}$ and $\mathbf{P}_2 = \mathbf{\Phi}_b^{(\mathrm{ov})}$, where $\mathbf{P}_1$ and $\mathbf{P}_3$ are square matrices of full rank.

2. Extended physical compatibility (Eqs. (21) and (30)), $\mathrm{rank}(\mathbf{W}_k) = n_b \ \forall \ k$ and $n_b = m^{(\mathrm{rem})}$:
   $\mathbf{P}_1 = \mathbf{\Phi}_b^{(\mathrm{rem})}$, $\mathbf{P}_2 = \mathbf{\Phi}_b^{(\mathrm{ov})}$ and $\mathbf{P}_3 = \mathbf{W}_k^\dagger \mathbf{\Phi}_g^{(\mathrm{par})}$, where $\mathbf{P}_1$ and $\mathbf{P}_3$ are square matrices of full rank.

3. Modal compatibility (Eqs. (22) and (25)) and $n_b > m^{(\mathrm{rem})}$:
   $\mathbf{P}_1 = \mathbf{P}_3 = \mathbf{I}^{(\mathrm{rem})}$ and $\mathbf{P}_2 = \mathbf{\Phi}_b^{(\mathrm{rem})\dagger} \mathbf{\Phi}_b^{(\mathrm{ov})}$, where $\mathbf{P}_1$ and $\mathbf{P}_3$ are square identity matrices.

The primal substructuring operator $\mathbf{L}_\mathrm{m}$ represents a null-space of $\mathbf{B}_\mathrm{m}$. This is a basis of independent vectors for which, when multiplied by $\mathbf{B}_\mathrm{m}$, a zero value is obtained. The number of such vectors is equal to the nullity of $\mathbf{B}_\mathrm{m}$. For all of the above-listed cases, the following symbolic null-space solution is considered[10]:

$$\mathbf{L}_\mathrm{m} = \begin{bmatrix} \mathbf{L}_\mathrm{m}^{(\mathrm{par})} \\ \mathbf{L}_\mathrm{m}^{(\mathrm{rem})} \\ \mathbf{L}_\mathrm{m}^{(\mathrm{ov})} \end{bmatrix} = \begin{bmatrix} \mathbf{P}_1^{-1}\mathbf{P}_2 \\ \mathbf{P}_1^{-1}\mathbf{P}_2 \\ \mathbf{I}^{(\mathrm{ov})} \end{bmatrix} \tag{35}$$

An analytical derivation following Eqs. (19) and (10) results in the primal modal mass matrix of the following form:[11]:

$$\tilde{\mathbf{M}}_\mathrm{m}^{(\mathrm{hyb})} = \begin{bmatrix} \mathbf{P}_1^{-1}\mathbf{P}_2 \\ \mathbf{P}_1^{-1}\mathbf{P}_2 \\ \mathbf{I}^{(\mathrm{ov})} \end{bmatrix}^\mathrm{T} \begin{bmatrix} \mathbf{I}^{(\mathrm{par})} & \mathbf{0} & \mathbf{0} \\ \mathbf{0} & -\mathbf{I}^{(\mathrm{rem})} & \mathbf{0} \\ \mathbf{0} & \mathbf{0} & \mathbf{I}^{(\mathrm{ov})} \end{bmatrix} \begin{bmatrix} \mathbf{P}_1^{-1}\mathbf{P}_2 \\ \mathbf{P}_1^{-1}\mathbf{P}_2 \\ \mathbf{I}^{(\mathrm{ov})} \end{bmatrix} = \mathbf{I}^{(\mathrm{ov})} \tag{36}$$

and analogously the primal modal damping and stiffness matrices read as:

$$\tilde{\mathbf{C}}_\mathrm{m}^{(\mathrm{hyb})} = 2\,\boldsymbol{\zeta}_r^{(\mathrm{ov})}\,\boldsymbol{\omega}_r^{(\mathrm{ov})}\,, \tag{37}$$

$$\tilde{\mathbf{K}}_\mathrm{m}^{(\mathrm{hyb})} = \boldsymbol{\omega}_r^{2\,(\mathrm{ov})}\,. \tag{38}$$

[10]Note that the null-space solution is not unique, however, this form appears to be convenient for further derivations. An equivalent solution can also be obtained by an arbitrary order change, linear combination, or non-zero scaling of the vector basis. For the determined M-SEMM type, the solution is independent of the matrix $\mathbf{P}_3$.

[11]Note, that the removed model is a sub-model of the parent model; therefore, they share an identical set of natural frequencies and damping ratios.

The dynamic properties (in terms of primal generalized coordinates) of the resulting hybrid model can be obtained by solving the eigenvalue problem:

$$\left(\tilde{\mathbf{K}}_{\mathrm{m}}^{(\mathrm{hyb})} - \boldsymbol{\lambda}^{(\mathrm{hyb})}\,\tilde{\mathbf{M}}_{\mathrm{m}}^{(\mathrm{hyb})}\right)\,\boldsymbol{\Phi}_{\xi}^{(\mathrm{hyb})} = \mathbf{0}\,, \tag{39}$$

with the trivial solution for hybrid eigenvalues $\boldsymbol{\lambda}^{(\mathrm{hyb})}$ and eigenvectors $\boldsymbol{\Phi}_{\xi}^{(\mathrm{hyb})}$ given as:

$$\boldsymbol{\lambda}^{(\mathrm{hyb})} = \boldsymbol{\omega}_r^{2\,(\mathrm{ov})}\,, \tag{40}$$

$$\boldsymbol{\Phi}_{\xi}^{(\mathrm{hyb})} = \mathbf{I}^{(\mathrm{ov})}\,. \tag{41}$$

This reveals that the hybrid model inherits the exact natural frequencies of the overlay model. Similarly, from the relation under the assumption of proportional viscous damping:

$$\begin{aligned}\boldsymbol{\Phi}_{\xi}^{(\mathrm{hyb})\,\mathrm{T}}\,\tilde{\mathbf{C}}_{\mathrm{m}}^{(\mathrm{hyb})}\,\boldsymbol{\Phi}_{\xi}^{(\mathrm{hyb})} &= 2\,\boldsymbol{\zeta}_r^{(\mathrm{hyb})}\,\boldsymbol{\omega}_r^{(\mathrm{hyb})}\,,\\ 2\,\boldsymbol{\zeta}_r^{(\mathrm{ov})}\,\boldsymbol{\omega}_r^{(\mathrm{ov})} &= 2\,\boldsymbol{\zeta}_r^{(\mathrm{hyb})}\,\boldsymbol{\omega}_r^{(\mathrm{hyb})}\,.\end{aligned} \tag{42}$$

Hence, the same stands for the exact equivalence of damping ratios: $\boldsymbol{\zeta}_r^{(\mathrm{hyb})} = \boldsymbol{\zeta}_r^{(\mathrm{ov})}$.
The eigenvectors $\boldsymbol{\Phi}_{\xi}^{(\mathrm{hyb})}$ are obtained in terms of unique generalized DOFs. Taking into account that the SEMM hybrid model is obtained at the parent-related DOFs and by considering the transformation from unique to dual generalized DOFs (Eq. (34)) and from dual generalized to physical DOFs (Eq. (18)), the hybrid mode shapes are obtained as:

$$\boldsymbol{\Phi}^{(\mathrm{hyb})} = \boldsymbol{\Phi}^{(\mathrm{par})}\,\mathbf{L}_{\mathrm{m}}^{(\mathrm{par})}\,\boldsymbol{\Phi}_{\xi}^{(\mathrm{hyb})} \tag{43}$$

which for all three above-listed $\mathbf{P}_1$ and $\mathbf{P}_2$ combinations within the determined case can be reformulated as[12]:

$$\begin{aligned}\boldsymbol{\Phi}^{(\mathrm{hyb})} &= \boldsymbol{\Phi}^{(\mathrm{par})}\,\boldsymbol{\Phi}_b^{(\mathrm{par})\dagger}\,\boldsymbol{\Phi}_b^{(\mathrm{ov})}\mathbf{I}^{(\mathrm{ov})}\\ &= \boldsymbol{\Phi}^{(\mathrm{par})}\,\boldsymbol{\Phi}_b^{(\mathrm{par})\dagger}\,\boldsymbol{\Phi}_b^{(\mathrm{ov})}\,.\end{aligned} \tag{44}$$

This derivation reveals that the determined M-SEMM type is analytically equivalent to SEREP (Eq. 15). This type of M-SEMM, therefore, does not represent a novel expansion technique; however, it provides an interesting substructuring-based interpretation of the established SEREP method.

4.3.2. Underdetermined type

This section presents the derivation of an under-determined M-SEMM type. In the modal domain such a case was already studied in the original presentation of SEREP [2]; however, it was considered to be of no practical use. Nonetheless, an effective methodology of the under-determined type in the modal domain could prove beneficial, as it would, for example, allow for a reduced experimental effort by reducing n_b and/or expanding the parent reduction basis by increasing $m^{(\mathrm{par})}$ in the expansion process of $m^{(\mathrm{ov})}$ mode shapes.

[12]For simplicity, the symbol for generalized inversion is also applied in the case of the classic inverse.

The basic and extended formulation are studied within the under-determined M-SEMM type, for both assuming $n_b < m^{(\mathrm{rem})}$:

1. The basic physical compatibility (Eqs. (21) and (24)):
   $\mathbf{P}_1 = \mathbf{P}_3 = \boldsymbol{\Phi}_b^{(\mathrm{rem})}$ and $\mathbf{P}_2 = \boldsymbol{\Phi}_b^{(\mathrm{ov})}$.

2. The extended physical compatibility (Eqs. (21) and (30)):
   $\mathbf{P}_1 = \boldsymbol{\Phi}_b^{(\mathrm{rem})}$, $\mathbf{P}_2 = \boldsymbol{\Phi}_b^{(\mathrm{ov})}$ and $\mathbf{P}_3 = \mathbf{W}_k^{\dagger}\,\boldsymbol{\Phi}_g^{(\mathrm{par})}$, where $\mathrm{rank}(\mathbf{P}_3) \leq n_b$, and $\mathbf{P}_3$ is mode-dependent in compliance with Eq. (29) and can also be (optionally) subjected to an additional TSVD-based weakening.

For the under-determined case, a convenient symbolic expression to evaluate the null-space of $\mathbf{B}_{\mathrm{m}}$ is the form [13]:

$$\mathbf{L}_{\mathrm{m}} = \begin{bmatrix} \mathbf{L}_{\mathrm{m}}^{(\mathrm{par})} \\ \mathbf{L}_{\mathrm{m}}^{(\mathrm{rem})} \\ \mathbf{L}_{\mathrm{m}}^{(\mathrm{ov})} \end{bmatrix} = \begin{bmatrix} \mathbf{P}_1^{\dagger}\,\mathbf{P}_2 & \mathrm{null}\,(\mathbf{P}_1) & \mathrm{null}\,(\mathbf{P}_3) \\ \mathbf{P}_1^{\dagger}\,\mathbf{P}_2 & \mathrm{null}\,(\mathbf{P}_1) & \mathbf{0} \\ \mathbf{I}^{(\mathrm{ov})} & \mathbf{0} & \mathbf{0} \end{bmatrix}. \tag{45}$$

As the number of columns in $\mathbf{L}_{\mathrm{m}}$ is clearly greater than $m^{(\mathrm{ov})}$, the resulting hybrid model will contain spurious modes. Therefore, additional measures to disregard the spurious part of the solution are introduced in the following.

Applying the proposed primal substructuring operator in further derivations using Eqs. (19) and (10), the primal modal mass matrix of the resulting hybrid model formulates as:

$$\begin{aligned} \tilde{\mathbf{M}}_{\mathrm{m}}^{(\mathrm{hyb})} &= \begin{bmatrix} \mathbf{P}_1^{\dagger}\,\mathbf{P}_2 & \mathrm{null}\,(\mathbf{P}_1) & \mathrm{null}\,(\mathbf{P}_3) \\ \mathbf{P}_1^{\dagger}\,\mathbf{P}_2 & \mathrm{null}\,(\mathbf{P}_1) & \mathbf{0} \\ \mathbf{I}^{(\mathrm{ov})} & \mathbf{0} & \mathbf{0} \end{bmatrix}^{\mathrm{T}} \begin{bmatrix} \mathbf{I}^{(\mathrm{par})} & \mathbf{0} & \mathbf{0} \\ \mathbf{0} & -\mathbf{I}^{(\mathrm{rem})} & \mathbf{0} \\ \mathbf{0} & \mathbf{0} & \mathbf{I}^{(\mathrm{ov})} \end{bmatrix} \begin{bmatrix} \mathbf{P}_1^{\dagger}\,\mathbf{P}_2 & \mathrm{null}\,(\mathbf{P}_1) & \mathrm{null}\,(\mathbf{P}_3) \\ \mathbf{P}_1^{\dagger}\,\mathbf{P}_2 & \mathrm{null}\,(\mathbf{P}_1) & \mathbf{0} \\ \mathbf{I}^{(\mathrm{ov})} & \mathbf{0} & \mathbf{0} \end{bmatrix} = \\ &= \left[\begin{array}{c:cc} \mathbf{I}^{(\mathrm{ov})} & \mathbf{0} & \left(\mathbf{P}_1^{\dagger}\,\mathbf{P}_2\right)^{\mathrm{T}}\,\mathbf{I}^{(\mathrm{par})}\,\mathrm{null}\,(\mathbf{P}_3) \\ \hdashline \mathbf{0} & \mathbf{0} & \mathrm{null}\,(\mathbf{P}_1)^{\mathrm{T}}\,\mathbf{I}^{(\mathrm{par})}\,\mathrm{null}\,(\mathbf{P}_3) \\ \mathrm{null}\,(\mathbf{P}_3)^{\mathrm{T}}\,\mathbf{I}^{(\mathrm{par})}\,\mathbf{P}_1^{\dagger}\,\mathbf{P}_2 & \mathrm{null}\,(\mathbf{P}_3)^{\mathrm{T}}\,\mathbf{I}^{(\mathrm{par})}\,\mathrm{null}\,(\mathbf{P}_1) & \mathrm{null}\,(\mathbf{P}_3)^{\mathrm{T}}\,\mathbf{I}^{(\mathrm{par})}\,\mathrm{null}\,(\mathbf{P}_3) \end{array}\right]. \end{aligned} \tag{46}$$

Similarly, the primal modal damping and stiffness matrices read as (for simplicity $\mathbf{C}_{\mathrm{m}}^{(\mathrm{s})} = 2\,\boldsymbol{\zeta}_r^{(\mathrm{s})}\,\boldsymbol{\omega}_r^{(\mathrm{s})}$ is introduced):

$$\tilde{\mathbf{C}}_{\mathrm{m}}^{(\mathrm{hyb})} = \left[\begin{array}{c:cc} \mathbf{C}_{\mathrm{m}}^{(\mathrm{ov})} & \mathbf{0} & \left(\mathbf{P}_1^{\dagger}\,\mathbf{P}_2\right)^{\mathrm{T}}\,\mathbf{C}_{\mathrm{m}}^{(\mathrm{par})}\,\mathrm{null}\,(\mathbf{P}_3) \\ \hdashline \mathbf{0} & \mathbf{0} & \mathrm{null}\,(\mathbf{P}_1)^{\mathrm{T}}\,\mathbf{C}_{\mathrm{m}}^{(\mathrm{par})}\,\mathrm{null}\,(\mathbf{P}_3) \\ \mathrm{null}\,(\mathbf{P}_3)^{\mathrm{T}}\,\mathbf{C}_{\mathrm{m}}^{(\mathrm{par})}\,\mathbf{P}_1^{\dagger}\,\mathbf{P}_2 & \mathrm{null}\,(\mathbf{P}_3)^{\mathrm{T}}\,\mathbf{C}_{\mathrm{m}}^{(\mathrm{par})}\,\mathrm{null}\,(\mathbf{P}_1) & \mathrm{null}\,(\mathbf{P}_3)^{\mathrm{T}}\,\mathbf{C}_{\mathrm{m}}^{(\mathrm{par})}\,\mathrm{null}\,(\mathbf{P}_3) \end{array}\right] \tag{47}$$

$$\tilde{\mathbf{K}}_{\mathrm{m}}^{(\mathrm{hyb})} = \left[\begin{array}{c:cc} \boldsymbol{\omega}_r^{2\,(\mathrm{ov})} & \mathbf{0} & \left(\mathbf{P}_1^{\dagger}\,\mathbf{P}_2\right)^{\mathrm{T}}\,\boldsymbol{\omega}_r^{2\,(\mathrm{par})}\,\mathrm{null}\,(\mathbf{P}_3) \\ \hdashline \mathbf{0} & \mathbf{0} & \mathrm{null}\,(\mathbf{P}_1)^{\mathrm{T}}\,\boldsymbol{\omega}_r^{2\,(\mathrm{par})}\,\mathrm{null}\,(\mathbf{P}_3) \\ \mathrm{null}\,(\mathbf{P}_3)^{\mathrm{T}}\,\boldsymbol{\omega}_r^{2\,(\mathrm{par})}\,\mathbf{P}_1^{\dagger}\,\mathbf{P}_2 & \mathrm{null}\,(\mathbf{P}_3)^{\mathrm{T}}\,\boldsymbol{\omega}_r^{2\,(\mathrm{par})}\,\mathrm{null}\,(\mathbf{P}_1) & \mathrm{null}\,(\mathbf{P}_3)^{\mathrm{T}}\,\boldsymbol{\omega}_r^{2\,(\mathrm{par})}\,\mathrm{null}\,(\mathbf{P}_3) \end{array}\right] \tag{48}$$

The hybrid modal parameters are again governed by the eigenvalue problem:

$$\left(\tilde{\mathbf{K}}_{\mathrm{m}}^{(\mathrm{hyb})} - \boldsymbol{\lambda}^{(\mathrm{hyb})}\,\tilde{\mathbf{M}}_{\mathrm{m}}^{(\mathrm{hyb})}\right)\,\boldsymbol{\Phi}_{\xi}^{(\mathrm{hyb})} = \mathbf{0}\,, \tag{49}$$

[13] To the best of the authors' knowledge, this analytical expression represents the null-space of the corresponding $\mathbf{B}_{\mathrm{m}}$ matrix for all physically meaningful sub-matrices $\mathbf{P}_1$, $\mathbf{P}_2$ and $\mathbf{P}_3$.

for which the eigenvalues represent solutions to the equation $\det\left(\tilde{\mathbf{K}}_{\mathrm{m}}^{(\mathrm{hyb})} - \boldsymbol{\lambda}^{(\mathrm{hyb})}\,\tilde{\mathbf{M}}_{\mathrm{m}}^{(\mathrm{hyb})}\right) = \mathbf{0}$. As indicated by the dotted lines in Eqs.(46) and (48), the matrix that is subjected to an evaluation of its determinant can be considered in the 2x2 block form as $\left[\begin{array}{c:c}\mathbf{E} & \mathbf{F}\\ \hdashline \mathbf{G} & \mathbf{H}\end{array}\right]$. According to the Schur complement [22], assuming $\mathbf{E} = \boldsymbol{\omega}_r^{2\,(\mathrm{ov})} - \boldsymbol{\lambda}^{(\mathrm{hyb})}\,\mathbf{I}^{(\mathrm{ov})}$ is a square, non-singular matrix, the expression in Eq. (49) can be rewritten in the form:

$$\det\left[\begin{array}{c:c}\mathbf{E} & \mathbf{F}\\ \hdashline \mathbf{G} & \mathbf{H}\end{array}\right] = \det\left[\mathbf{E}\right]\,\det\left[\mathbf{H} - \mathbf{G}\,\mathbf{E}^{-1}\,\mathbf{F}\right] = \mathbf{0}\,. \tag{50}$$

Thereby, an independent solution to the part of equation $\det\left[\mathbf{E}\right] = \det\left(\boldsymbol{\omega}_r^{2\,(\mathrm{ov})} - \boldsymbol{\lambda}^{(\mathrm{hyb})}\,\mathbf{I}^{(\mathrm{ov})}\right) = \mathbf{0}$ reveals that the exact overlay model's eigenvalues are always present as a part of the full solution to the corresponding eigenvalue problem. This observation justifies the possibility of applying mode-dependent constraints in the extended formulation, proposed in Eq. (29).

Since we are only interested in acquiring the hybrid mode shapes that correspond to the overlay model's eigenvalues, while the rest of the solutions are considered to be spurious, the process of solving the eigenvectors translates to a null-space evaluation in the form:

$${}_k\boldsymbol{\phi}_{\xi}^{(\mathrm{hyb})} = \mathrm{null}\left(\tilde{\mathbf{K}}_{\mathrm{m}}^{(\mathrm{hyb})} - \omega_k^{2\,(\mathrm{ov})}\,\tilde{\mathbf{M}}_{\mathrm{m}}^{(\mathrm{hyb})}\right);\quad k = 1,\ldots,m^{(\mathrm{ov})}\,. \tag{51}$$

Note that in the extended formulation, also $\tilde{\mathbf{M}}_{\mathrm{m}}^{(\mathrm{hyb})}$ and $\tilde{\mathbf{K}}_{\mathrm{m}}^{(\mathrm{hyb})}$ are re-evaluated for each k due to the mode-dependent decoupling weakening basis $\mathbf{W}_k$.

In this way we can successfully disregard the spuriousities in the hybrid model. Nevertheless, a possible concern arises if an eigenvalue corresponding to the spurious mode exactly matches any of the overlay model's eigenvalues. Then, a possible way to separate the spurious and the proper hybrid mode shape is to compare them to the corresponding overlay mode shape (using, e.g., the modal assurance criterion (MAC) [23]). A high level of the correlation between the boundary DOFs of the sought hybrid mode shape and the corresponding overlay mode shape is expected, thus making it possible to disregard a potentially spurious solution.

Given this filtered eigenvector solution, it transpires that the corresponding damping ratios of the hybrid model are also retained:

$$\zeta_k^{(\mathrm{hyb})} = \zeta_k^{(\mathrm{ov})};\quad k = 1,\ldots,m^{(\mathrm{ov})}\,. \tag{52}$$

The hybrid mode shapes are obtained in compliance with the transformations in Eqs. (18) and (34), considering the parent-related DOFs of the assembled system:

$${}_k\boldsymbol{\phi}^{(\mathrm{hyb})} = \boldsymbol{\Phi}^{(\mathrm{par})}\,\mathbf{L}_{\mathrm{m}}^{(\mathrm{par})}\,{}_k\boldsymbol{\phi}_{\xi}^{(\mathrm{hyb})};\quad k = 1,\ldots,m^{(\mathrm{ov})}\,. \tag{53}$$

Again, note that in the extended formulation $\mathbf{L}_{\mathrm{m}}^{(\mathrm{par})}$ is also mode dependent.

The proposed methodology for an under-determined case represents a novel expansion technique. Given that the from of Eq. (53) is similar to Eq. (15), this technique can also be interpreted as a potentially useful variation of the under-determined type of SEREP [2].

5. Numerical example

In this section the proposed M-SEMM methodology is applied to a numerical example and compared to the established techniques SEMM and SEREP[14].

[14]Note that in the following, SEMM is denoted as the original frequency-based implementation and M-SEMM is only considered for the under-determined type as the determined type is analytically equivalent to SEREP.

This example simulates the typical numerical-experimental modelling of a component. The overlay model is a beam-like structure having 16 cylindrical holes, with two of them used for the fixed mounting, as depicted in Fig. 5a. The parent model represents its approximate numerical counterpart, which is geometrically simplified by neglecting the holes, and the fixed boundary conditions are applied at the surfaces near the actual mounting holes (Fig. 5b). For the overlay model the material properties of an aluminium alloy with a Young's modulus of 72 GPa and a density of 2770 kg/m^3 are adopted. Compared to these, a 5% lower density and a 5% higher Young's modulus are adopted for the parent model. The modal damping ratios for all the modes of the overlay and parent models are defined as 0.5% and 0.3%, respectively.

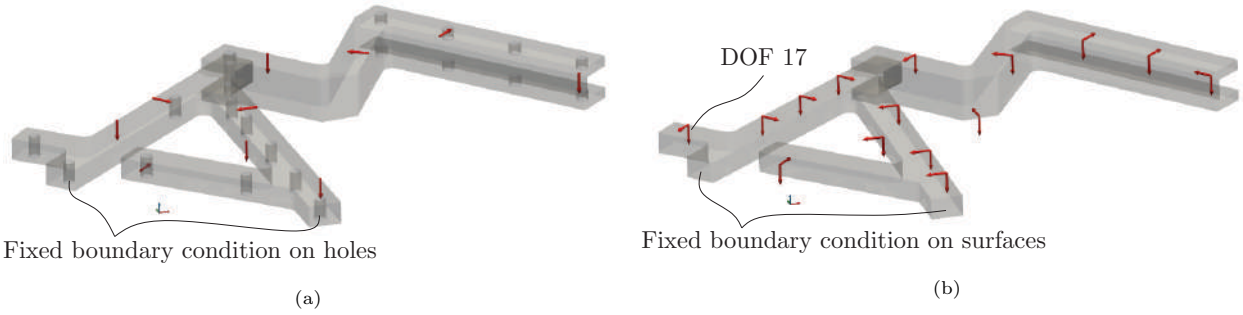

Figure 5: Equivalent models: (a) Overlay model; (b) Parent model with simplified geometry, boundary conditions and approximated material properties.

The frequency range up to 2 kHz is considered, corresponding to the first 15 overlay model's natural modes[15]. The size of the dense set of parent's DOFs is $n_g = 30$, while for the sparse set of overlay's DOFs the size is $n_b = 10$. The corresponding (collocated) input and output locations are denoted by the red arrows (Fig. 5).

Given the number of sparse DOFs, for SEREP the dimension of the parent model's modal basis is limited to $m^{(\mathrm{par})} \leq n_b$. The proposed under-determined M-SEMM type; however, allows for the use of a richer expansion basis ($m^{(\mathrm{par})} > n_b$).

For example, let us consider the parent modal basis of sizes $m^{(\mathrm{par})} = 9$ and $m^{(\mathrm{par})} = 25$ for the SEREP and M-SEMM methods, respectively, and perform the expansion of 15 overlay model's mode shapes. In Fig. 6, the resulting hybrid mode shapes, obtained from the SEREP, the basic M-SEMM and the extended M-SEMM are compared to the reference using the modal assurance criterion (MAC) [23].

For the given case, Fig. 6a demonstrates the apparent limitation of the SEREP, for which, due to the reduced parent modal basis, the expansion is only successful for the first 9 hybrid modes. On the other hand, (at least for the higher modes) a significantly better performance of both the basic and extended M-SEMM formulations is evident form Figs. 6b and 6c.

A similar expansion process is performed for different $m^{(\mathrm{par})}$ values. A diagram in Fig. 7 depicts the average diagonal values of the corresponding MAC matrices. The results show that when considering an overlay model, for which the number of physical DOFs is lower than the number of its modes, using a richer parent model's modal basis is beneficial for the performance of the expansion process.

A comparison of the M-SEMM and the frequency-based SEMM methodology is performed in terms of the frequency-response functions (FRFs). To ensure equivalent input data for both methods, the admittance matri-

[15]Generally, it is reasonable to expect that a parent model's modal basis with an equal or greater number of vectors will be required to expand all 15 modes of the overlay model.

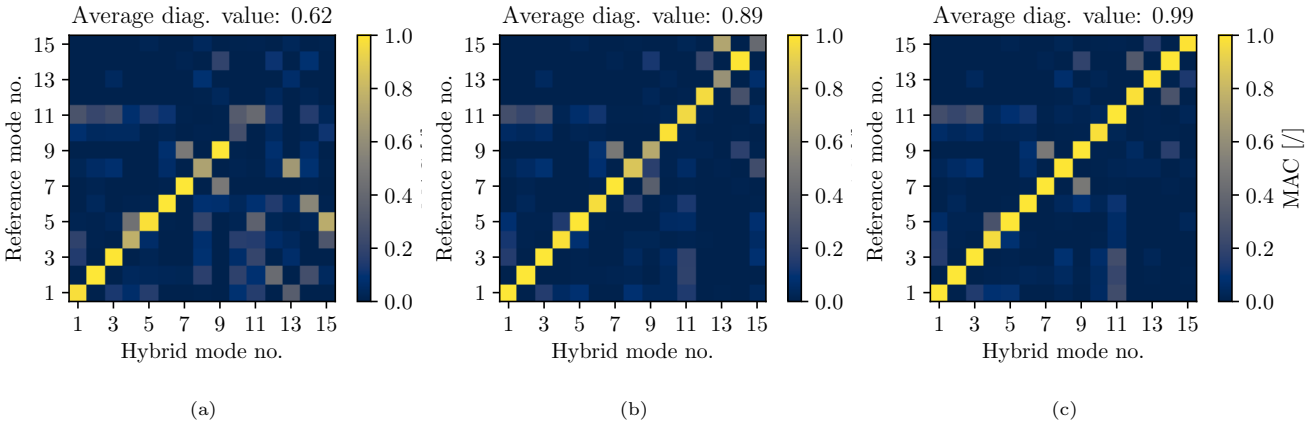

Figure 6: MAC matrix: (a) SEREP; (b) M-SEMM - basic formulation (c) M-SEMM - extended formulation.

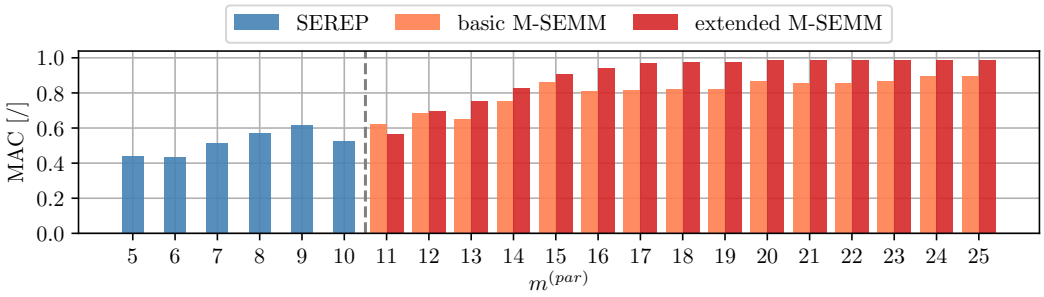

Figure 7: Average diagonal values of MAC matrices with regard to the changing value of $m^{(\mathrm{par})}$.

ces are obtained by modal superposition, considering the first $m^{(\mathrm{par})} = 25$ and $m^{(\mathrm{ov})} = 15$ modal contributions for the parent and overlay models, respectively. To quantify the agreement between the acquired FRFs, an amplitude and phase-sensitive coherence criterion [24] is adopted.

The results of the expansion process applying basic formulations of the SEMM and M-SEMM are given in Fig. 8. A comparison of the driving-point FRFs in DOF 17 (Fig. 5b) is considered, whereas the description in the title provides the average coherence value for the full receptance matrix.

The frequency-based results in Fig. 8a have a high incidence of spuriousities, which is a known limitation of the basic SEMM [8]. A comparison with the basic M-SEMM results in Fig. 8b demonstrates the ability of M-SEMM to filter-out spurious modes. However, a similar average coherence of the full receptance matrix is achieved for both methodologies.

The extended formulation in the frequency domain, however, typically effectively eliminates the problem of spurious modes, as is evident in Fig. 9a. Compared to the results of the extended M-SEMM formulation, the hybrid results are very similar, both exhibiting a high level of agreement with the reference.

This numerical example demonstrates the applicability of M-SEMM, which appears to be a potentially useful extension to the SEREP method for the expansion of spatially sparse overlay models.

The comparison between the modal and frequency-based implementations of SEMM implies possible differences in the outcome, even when considering purely numerical models, which can be mainly attributed to the per-frequency-line or per-mode types of operation.

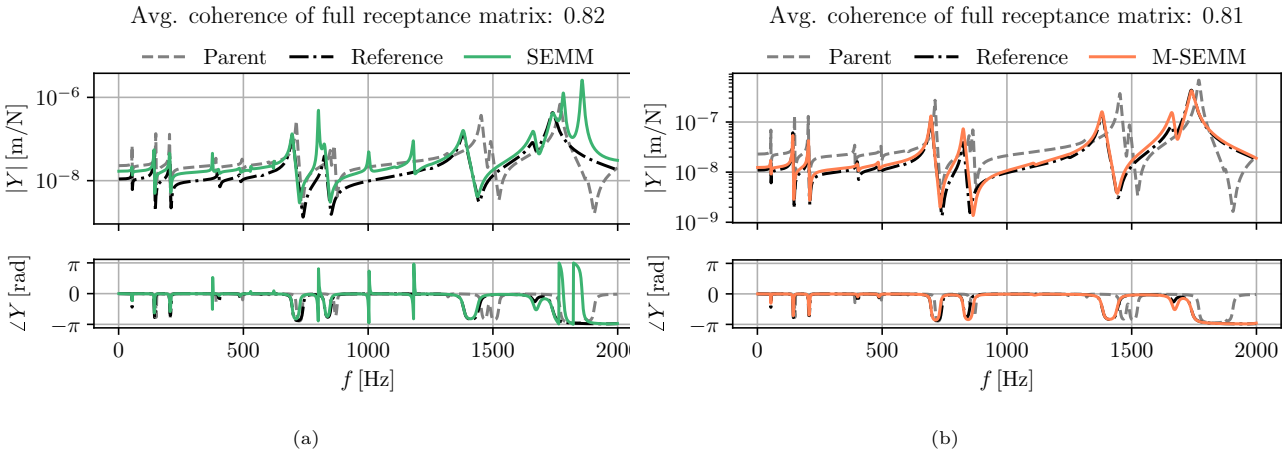

(a) (b)

Figure 8: Basic formulation - DOF 17 driving point FRF: (a) SEMM; (b) M-SEMM.

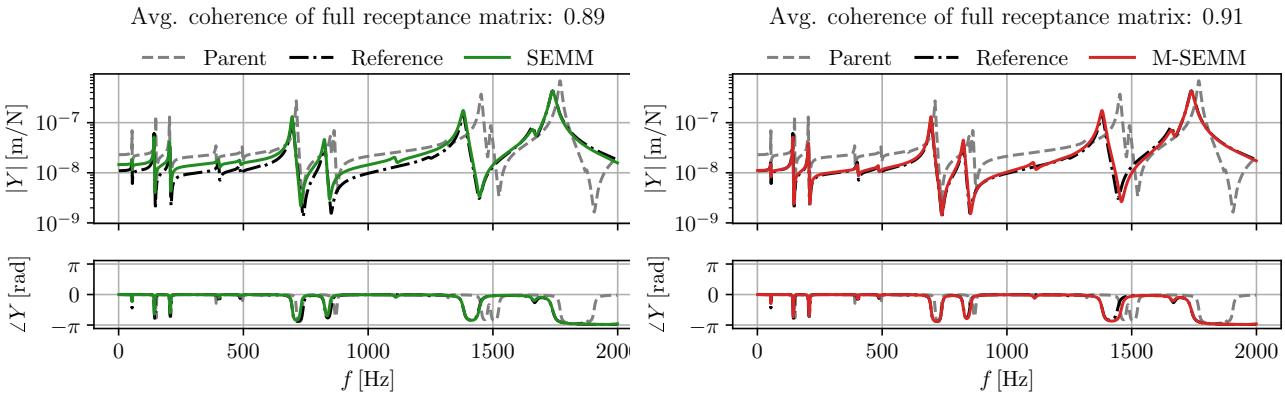

(a) (b)

Figure 9: Extended formulation - DOF 17 driving-point FRF : (a) SEMM; (b) M-SEMM.

6. Experimental example

An experimental study was performed on a solid aluminium beam with dimensions of $15 \times 40 \times 500$ mm^3, as shown in Fig. 10a. Two grooves were milled to half of the beam height over the full width. Approximately fixed boundary conditions were provided using a bolted connection through a rubber padding. A modal hammer PCB-086E80 was used to excite the structure at 29 equidistant points, as depicted in Fig. 10b. The response was measured at four locations (points 4, 12, 20 and 28) using Dytran 3097A1 uniaxial translational accelerometers. A full 4×29 admittance matrix represents a reference to be compared with the hybrid models, whereas an arbitrary sub-model can be considered as an overlay model.

The modal identification was performed using a poly-reference algorithm [25] in the frequency range up to 5 kHz, which corresponds to the first seven natural modes. Note, that for real-life structures a deviation between the measured and reconstructed FRFs is not negligible (a correlation of 93% is reported in [25]), even when using state-of-the-art modal identification algorithms. Such a discrepancy could prevail over the performance differences between the frequency- and modal-based methodologies. Therefore, a fairly simple experimental model was acquired for which the average coherence between the measured and the reconstructed receptance matrix is 97%. All the result comparisons in this section are made in terms of FRFs to provide a comparison between all the methods.

The parent model is a 2D finite-element model of a cantilever beam, simplified in terms of geometry by disregarding the grooves and with approximated boundary conditions, as depicted in Fig. 10b. An aluminium alloy material's properties are adopted with a Young's modulus of 75.6 GPa and a density of 2631.5 kg/m^3. The modal damping ratio for all the parent model's modes is 0.3%.

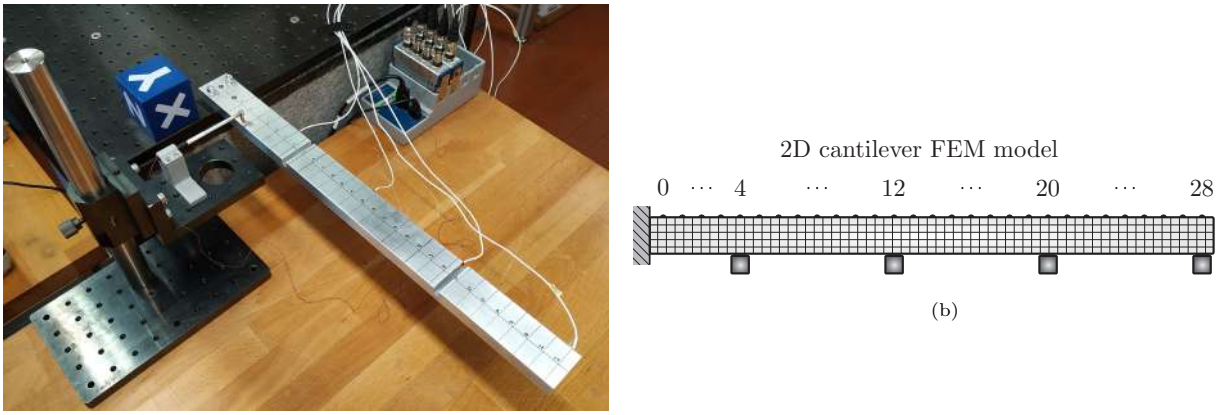

(a) (b)

Figure 10: Experimental case: (a) Experimental setup; (b) Parent model as a 2D cantilever beam FEM model.

To perform the expansion of $m^{(\mathrm{ov})} = 7$ overlay model's mode shapes with SEREP, a set of $m^{(\mathrm{par})} = 7$ parent's mode shapes and $n_b = 8$ experimental points are considered at locations $[0, 4, 8, 12, 16, 20, 24, 28]$. Such an overlay model is expanded to the $n_g = 29$ parent model's locations. By performing modal superposition of the hybrid modal parameters, a resulting FRF (input-output location 10–2) is given in Fig. 11a. The comparison of the full hybrid and experimental admittance is depicted in a coherence diagram for all the input-output locations in Fig. 11b. A fairly good agreement with the reference is obtained with an average coherence of 0.92.

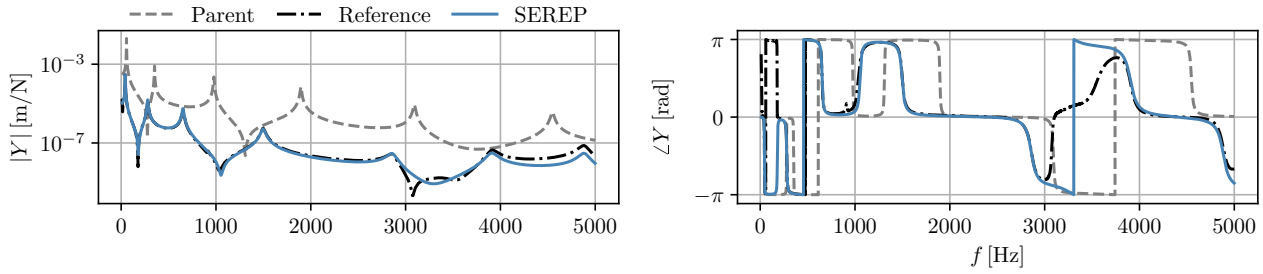

(a)

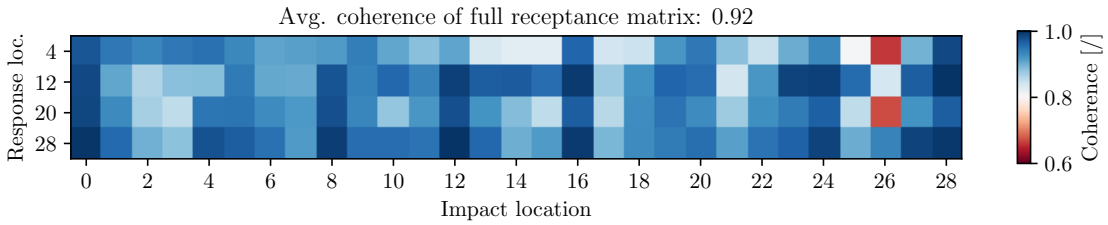

(b)

Figure 11: SEREP - hybrid model ($n_b = 8$ experimental locations): (a) $\mathbf{Y}_{10,2}$; (b) Average coherence values for the full receptance matrix.

A similar expansion process is performed with the SEMM; however, the number of experimental locations is reduced by half. The locations $[4, 12, 20, 28]$ are considered to obtain a 4×4 overlay model's admittance matrix

and the extended formulation of the SEMM is performed in the frequency domain to obtain a hybrid model. Despite the significant reduction in the number of experimental locations, the FRF in Fig. 12b shows a high level of agreement with the reference. However, it also exhibits a rare occurrence of spuriousities in the extended SEMM hybrid model. The average coherence value of the full hybrid admittance matrix in Fig. 12b is 0.82.

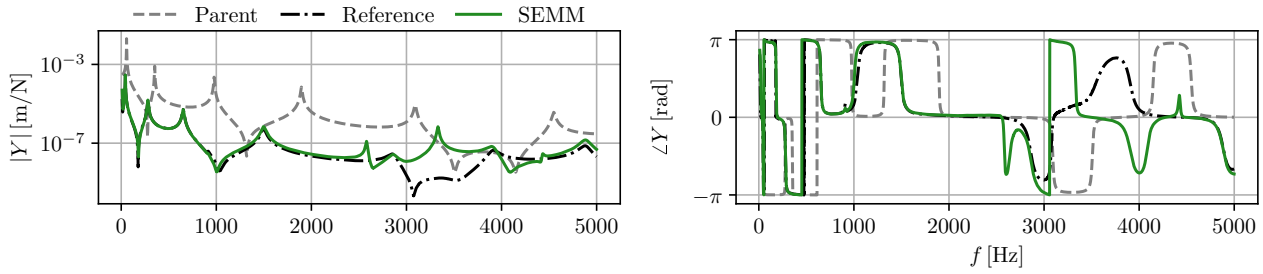

(a)

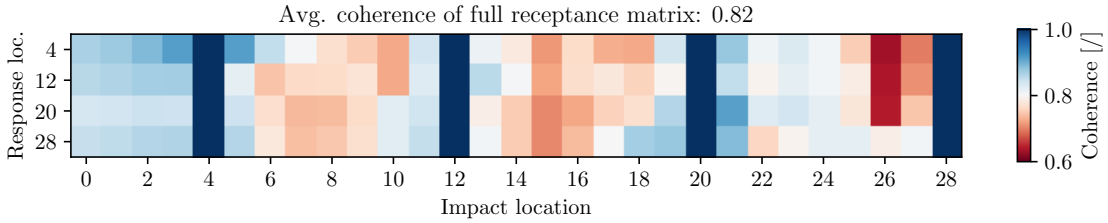

(b)

Figure 12: SEMM - hybrid model (n_b = 4 experimental locations): (a) $\mathbf{Y}_{10,2}$; (b) Average coherence values for full receptance matrix.

The expansion is repeated with the extended M-SEMM by considering the same $n_b = 4$ experimental points for the overlay model's modal parameters. The hybrid model is obtained by modal superposition with the resulting FRF shown in Fig. 12b. A comparison to the frequency-based result in Fig. 12b reveals that spuriousities are successfully filtered out and the agreement with the experimental reference is slightly higher.

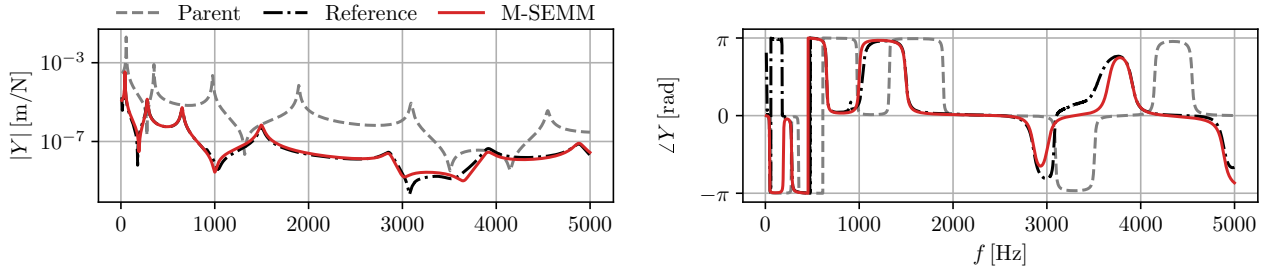

(a)

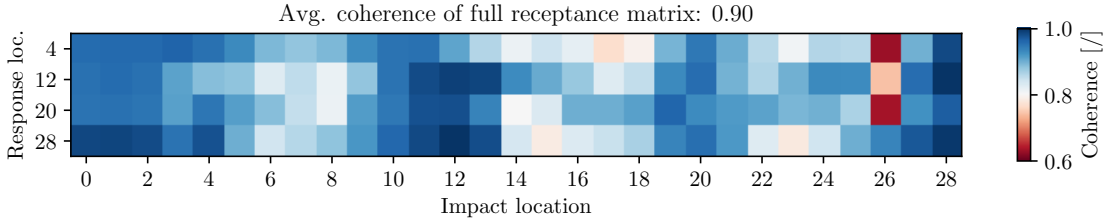

(b)

Figure 13: M-SEMM - hybrid model (n_b = 4 experimental locations): (a) $\mathbf{Y}_{10,2}$; (b) Average coherence values for full receptance matrix.

The average coherence value of the full hybrid admittance matrix in Fig. 13b is 0.90. In this case, compared with the performance of the SEREP in Fig. 11b, M-SEMM is able to provide a comparable result by considering a substantially sparser overlay model. In a real-life application this can be seen as an important advantage, as it allows for a smaller effort in the experimental evaluation of the overlay model.

7. Conclusion

This paper introduces an expansion method called M-SEMM, a reformulation of the frequency-based SEMM in the modal domain.

The proposed methodology distinguishes between different versions. Among them, a theoretical derivation of the under-determined M-SEMM type reveals its equivalence to the system equivalent reduction expansion process (SEREP), a well-established reduction/expansion method. The corresponding derivation can also be seen as a substructuring-based interpretation of the SEREP.

The under-determined type of M-SEMM represents a novel expansion method in the modal domain, which can be further divided into a basic and an extended formulation. This type of methodology can be seen as a potentially useful extension of the SEREP, applicable when considering sparse models with a high modal density.

A comparison of the expanded models in a numerical study shows similar results for the frequency-based and modal implementation. However, the strong point of M-SEMM appears to be its superior ability to filter out spuriousities from the hybrid models.

In the experimental study on a lightly damped structure, the M-SEMM expanded model demonstrates a significantly higher level of agreement with the reference, compared to the frequency-based method. The obtained results are also comparable with the outcome of the SEREP method with double the number of required experimental points.

The presented examples are performed on academic structures and are intended for validation and comparison of the proposed method with existing expansion techniques. Future work will focus on the applicability of the proposed methodology to complex real-life structures.

An interested reader may also be interested in a Python-based implementation of the proposed M-SEMM method, which is a part of an open-source package pyFBS [26].

Acknowledgements

The authors acknowledge partial financial support from the core research funding P2-0263 and the applied research project L2-1837, both financed by ARRS, the Slovenian research agency.

Appendix A. Alternative derivation of the extended LM-FBS SEMM formulation

This appendix is dedicated to the interpretation of an extended decoupling interface in frequency-based SEMM. First, a brief overview of the Lagrange-multiplier frequency-based substructuring (LM-FBS) is provided, followed by the alternative derivation of the extended SEMM formulation.

Appendix A.1. Brief overview of LM-FBS

Referring back to Eqs. (2)–(4) and transforming them to the frequency domain, we obtain:

$$\boldsymbol{u} = \mathbf{Y}\,(\boldsymbol{f} + \boldsymbol{g})\,, \tag{A.1}$$

$$\mathbf{B}\,\boldsymbol{u} = \mathbf{0}, \tag{A.2}$$

$$\mathbf{L}^{\mathrm{T}}\boldsymbol{g} = \mathbf{0}, \tag{A.3}$$

where $\mathbf{Y}$ is the uncoupled (block-diagonal) admittance of the substructures' admittances. The equilibrium conditions are fulfilled by introducing the Lagrange multiplier vector $\boldsymbol{\lambda}$, which translates Eq. (A.3) into:

$$\boldsymbol{g} = -\mathbf{B}^{\mathrm{T}}\,\boldsymbol{\lambda}. \tag{A.4}$$

Solving the set of Eqs. (A.1), (A.2) and (A.4) while eliminating the Lagrange multiplier vector yields the response of the assembled system:

$$\boldsymbol{u} = \widetilde{\mathbf{Y}}\,\boldsymbol{f} = \left[\mathbf{Y} - \mathbf{Y}\,\mathbf{B}^{\mathrm{T}}\left(\mathbf{B}\,\mathbf{Y}\,\mathbf{B}^{\mathrm{T}}\right)^{-1}\mathbf{B}\,\mathbf{Y}\right]\boldsymbol{f}. \tag{A.5}$$

Hence, the admittance of the assembled model can be expressed as:

$$\widetilde{\mathbf{Y}} = \mathbf{Y} - \mathbf{Y}\,\mathbf{B}^{\mathrm{T}}\left(\mathbf{B}\,\mathbf{Y}\,\mathbf{B}^{\mathrm{T}}\right)^{-1}\mathbf{B}\,\mathbf{Y}. \tag{A.6}$$

Appendix A.2. SEMM - extended formulation

The uncoupled admittance matrix (following the concepts presented in Sec. 3.2) for the fully-extended SEMM reads as:

$$\mathbf{Y} = \left[\begin{array}{cc|cc|c} \mathbf{Y}_{ii}^{(\mathrm{par})} & \mathbf{Y}_{ib}^{(\mathrm{par})} & \mathbf{0} & \mathbf{0} & \mathbf{0} \\ \mathbf{Y}_{bi}^{(\mathrm{par})} & \mathbf{Y}_{bb}^{(\mathrm{par})} & \mathbf{0} & \mathbf{0} & \mathbf{0} \\ \hline \mathbf{0} & \mathbf{0} & -\mathbf{Y}_{ii}^{(\mathrm{rem})} & -\mathbf{Y}_{ib}^{(\mathrm{rem})} & \mathbf{0} \\ \mathbf{0} & \mathbf{0} & -\mathbf{Y}_{bi}^{(\mathrm{rem})} & -\mathbf{Y}_{bb}^{(\mathrm{rem})} & \mathbf{0} \\ \hline \mathbf{0} & \mathbf{0} & \mathbf{0} & \mathbf{0} & \mathbf{Y}_{bb}^{(\mathrm{ov})} \end{array}\right]. \tag{A.7}$$

Coupling the compatibility condition between the equivalent models is given as:

$$\boldsymbol{u}_b^{(\mathrm{rem})} = \boldsymbol{u}_b^{(\mathrm{ov})} \tag{A.8}$$

while the extended decoupling compatibility[16] reads as:

$$\boldsymbol{u}_g^{(\mathrm{par})} = \boldsymbol{u}_g^{(\mathrm{rem})}\,. \tag{A.9}$$

[16] By extending the decoupling interface from boundary to the full set of DOFs, the interface observability and controllability is improved, which is beneficial for the efficiency of the decoupling procedure.

The corresponding $\mathbf{B}$ matrix takes the following form:

$$\mathbf{B} = \left[\begin{array}{cc|cc|c} \mathbf{0} & \mathbf{0} & \mathbf{0} & \mathbf{I} & -\mathbf{I} \\ \hline \multicolumn{2}{c|}{\mathbf{I}} & \multicolumn{2}{c|}{-\mathbf{I}} & \mathbf{0} \end{array}\right]. \tag{A.10}$$

Hence, compatibility and the equilibrium conditions are enforced on all the collocated DOFs. If we express the interface flexibility matrix from Eqs. (A.6), (A.7) and (A.10):

$$\mathbf{Y}_{\text{int}} = \mathbf{B}\,\mathbf{Y}\,\mathbf{B}^{\text{T}} = \left[\begin{array}{cc} -\mathbf{Y}_{bb}^{(\text{rem})} + \mathbf{Y}_{bb}^{(\text{ov})} & \mathbf{Y}_{bg}^{(\text{rem})} \\ \mathbf{Y}_{gb}^{(\text{rem})} & \mathbf{0} \end{array}\right]_{(n_b+n_g)\times(n_b+n_g)} \tag{A.11}$$

we can see that the problem is indeterminate as the $\mathbf{Y}_{\text{int}}$ matrix is singular with rank $2\,n_b$. This results in the inapplicability of its direct inversion. By applying a generalized inverse instead, the corresponding singular-value truncation can be interpreted as a weakening of the decoupling compatibility and equilibrium conditions (see Appendix C in [27]). The effects of the generalized inverse can be replicated by performing a projection of the extended compatibility and equilibrium conditions to the sub-space of the removed model, as discussed in Appendix B in [27]. The corresponding weakening matrix is given as:

$$\mathbf{W}^{\dagger} = \begin{bmatrix} \mathbf{I} & \mathbf{0} \\ \mathbf{0} & \mathbf{Y}_{gb}^{(\text{rem})\dagger} \end{bmatrix}, \tag{A.12}$$

for which the weakened compatibility condition in the original DOFs space reads as:

$$\mathbf{W}^{\dagger}\,\mathbf{B}\,\boldsymbol{u} = \left[\begin{array}{cc|cc|c} \mathbf{0} & \mathbf{0} & \mathbf{0} & \mathbf{I} & -\mathbf{I} \\ \hline \multicolumn{2}{c|}{\mathbf{Y}_{gb}^{(\text{rem})\dagger}} & \multicolumn{2}{c|}{-\mathbf{Y}_{gb}^{(\text{rem})\dagger}} & \mathbf{0} \end{array}\right] \boldsymbol{u}. \tag{A.13}$$

The same basis is also applied to weaken the equilibrium conditions:

$$\boldsymbol{g} = -\mathbf{B}^{\text{T}}\left(\mathbf{W}^{\dagger}\right)^{\text{T}}\boldsymbol{\lambda}_m = \left[\begin{array}{c|c} \mathbf{0} & \mathbf{Y}_{bg}^{(\text{rem})\dagger} \\ \mathbf{0} & \\ \hline \mathbf{0} & -\mathbf{Y}_{bg}^{(\text{rem})\dagger} \\ \mathbf{I} & \\ \hline -\mathbf{I} & \mathbf{0} \end{array}\right] \boldsymbol{\lambda}_m, \tag{A.14}$$

where $\boldsymbol{\lambda}_m$ are the interface forces in the reduced space. Using the above-defined compatibility and equilibrium conditions the assembled admittance becomes:

$$\widetilde{\mathbf{Y}} = \mathbf{Y} - \mathbf{Y}\,\mathbf{B}^{\text{T}}\left(\mathbf{W}^{\dagger}\right)^{\text{T}}\left(\mathbf{W}^{\dagger}\mathbf{B}\mathbf{Y}\mathbf{B}^{\text{T}}\left(\mathbf{W}^{\dagger}\right)^{\text{T}}\right)^{-1}\mathbf{W}^{\dagger}\mathbf{B}\,\mathbf{Y}. \tag{A.15}$$

Now, the interface flexibility matrix in the reduced space

$$\mathbf{Y}_{\text{int}} = \mathbf{W}^{\dagger}\mathbf{B}\mathbf{Y}\mathbf{B}^{\text{T}}\left(\mathbf{W}^{\dagger}\right)^{\text{T}} = \begin{bmatrix} -\mathbf{Y}_{bb}^{(\text{rem})} + \mathbf{Y}_{bb}^{(\text{ov})} & \mathbf{I} \\ \mathbf{I} & \mathbf{0} \end{bmatrix}_{2\,n_b\times 2\,n_b} \tag{A.16}$$

is of rank $2\,n_b$ and thus invertible. By expressing the inverse of the 2x2 block matrix [22] $\mathbf{Y}_{\text{int}}$, we obtain:

$$\left(\mathbf{W}^{\dagger}\mathbf{B}\mathbf{Y}\mathbf{B}^{\text{T}}\left(\mathbf{W}^{\dagger}\right)^{\text{T}}\right)^{-1} = \begin{bmatrix} \mathbf{0} & \mathbf{I} \\ \mathbf{I} & \mathbf{Y}_{bb}^{(\text{rem})} - \mathbf{Y}_{bb}^{(\text{ov})} \end{bmatrix}, \tag{A.17}$$

from which the following conclusion can be made: it is evident that the overlay model $\mathbf{Y}^{(\mathrm{ov})}$ which provides the dynamic properties of the hybrid model is not inverted in the process, which is treated as a strong point of the SEMM method [8].

With the inverse of the interface flexibility matrix known, Eq. (A.15) is employed to obtain the admittance of the hybrid model. For the sake of simplicity, one can only focus on the first two rows and columns of the $\mathbf{Y}^{(\mathrm{hyb})}$, thus exploiting the nature of LM-FBS for which the interface DoFs are repeated in the assembled result:

$$\mathbf{Y}^{(\mathrm{hyb})} = \begin{bmatrix} \mathbf{Y}_{ii}^{(\mathrm{par})} & \mathbf{Y}_{ib}^{(\mathrm{par})} \\ \mathbf{Y}_{bi}^{(\mathrm{par})} & \mathbf{Y}_{bb}^{(\mathrm{par})} \end{bmatrix} - \tag{A.18}$$

$$- \begin{bmatrix} \mathbf{Y}_{ii}^{(\mathrm{par})} & \mathbf{Y}_{ib}^{(\mathrm{par})} \\ \mathbf{Y}_{bi}^{(\mathrm{par})} & \mathbf{Y}_{bb}^{(\mathrm{par})} \end{bmatrix} \left(\begin{bmatrix} \mathbf{Y}_{bi}^{(\mathrm{rem})} & \mathbf{Y}_{bb}^{(\mathrm{rem})} \end{bmatrix} \right)^{\dagger} \left(\mathbf{Y}_{bb}^{(\mathrm{rem})} - \mathbf{Y}_{bb}^{(\mathrm{ov})} \right) \left(\begin{bmatrix} \mathbf{Y}_{ib}^{(\mathrm{rem})} \\ \mathbf{Y}_{bb}^{(\mathrm{rem})} \end{bmatrix} \right)^{\dagger} \begin{bmatrix} \mathbf{Y}_{ii}^{(\mathrm{par})} & \mathbf{Y}_{ib}^{(\mathrm{par})} \\ \mathbf{Y}_{bi}^{(\mathrm{par})} & \mathbf{Y}_{bb}^{(\mathrm{par})} \end{bmatrix}. \tag{A.19}$$

Simplifying the expression above, the single-line equation for the extended SEMM is expressed as:

$$\mathbf{Y}^{(\mathrm{hyb})} = \mathbf{Y}_{gg}^{(\mathrm{par})} - \mathbf{Y}_{gg}^{(\mathrm{par})} \mathbf{Y}_{bg}^{(\mathrm{rem})\,\dagger} \left(\mathbf{Y}_{bb}^{(\mathrm{rem})} - \mathbf{Y}_{bb}^{(\mathrm{ov})} \right) \mathbf{Y}_{gb}^{(\mathrm{rem})\,\dagger} \mathbf{Y}_{gg}^{(\mathrm{par})}. \tag{A.20}$$

References

[1] R. J. Guyan, Reduction of stiffness and mass matrices, AIAA journal 3 (2) (1965) 380–380.

[2] J. C. O'Callahan, P. Avitabile, R. Riemer, System equivalent reduction expansion process (SEREP), in: Proceedings of the VII International Modal Analysis Conference (IMAC), Vol. 1, Society for Experimental Mechanics, 1989, pp. 29–37.

[3] L. Thibault, A. Butland, P. Avitabile, Variability improvement of key inaccurate node groups–VIKING, in: Topics in Modal Analysis II, Volume 6, Springer, 2012, pp. 603–624.

[4] Y. Chen, B. Zhang, S. Chen, Model reduction technique tailored to the dynamic analysis of a beam structure under a moving load, Shock and Vibration 2014 (2014).

[5] J. Baqersad, P. Poozesh, C. Niezrecki, P. Avitabile, Photogrammetry and optical methods in structural dynamics–a review, Mechanical Systems and Signal Processing 86 (2017) 17–34.

[6] Y. Chen, D. Joffre, P. Avitabile, Underwater dynamic response at limited points expanded to full-field strain response, Journal of Vibration and Acoustics 140 (5) (2018).

[7] Y. Chen, P. Logan, P. Avitabile, J. Dodson, Non-model based expansion from limited points to an augmented set of points using Chebyshev polynomials, Experimental Techniques 43 (5) (2019) 521–543.

[8] S. W. Klaassen, M. V. van der Seijs, D. de Klerk, System equivalent model mixing, Mechanical Systems and Signal Processing 105 (2018) 90–112.

[9] S. Klaassen, M. van der Seijs, Introducing SEMM: A novel method for hybrid modelling, in: Dynamics of Coupled Structures, Volume 4, Springer, 2018, pp. 117–125.

[10] S. Klaassen, D. Rixen, The inclusion of a singular-value based filter in SEMM, in: Proceedings of the 38th International Modal Analysis Conference, A Conference on Structural Dynamics, 2020.

[11] E. Pasma, S. Klaassen, L. Nieuwenhuijse, M. Van Der Seijs, D. Lennström, Application of system equivalent model mixing (SEMM) to model the structural dynamic properties of a complex vehicle component using numerical and experimental data, Proceedings of ISMA2018 (2018).

[12] Z. Saeed, S. W. Klaassen, C. M. Firrone, T. M. Berruti, D. J. Rixen, Experimental joint identification using system equivalent model mixing in a bladed disk, Journal of Vibration and Acoustics 142 (5) (2020) 051001.

[13] S. Klaassen, D. Rixen, Using SEMM to identify the joint dynamics in multiple degrees of freedom without measuring interfaces, in: Dynamic Substructures, Volume 4, Springer, 2020, pp. 87–99.

[14] T. Bregar, K. Zaletelj, G. Čepon, J. Slavič, M. Boltežar, Full-field FRF estimation from noisy high-speed-camera data using a dynamic substructuring approach, Mechanical Systems and Signal Processing 150 (2021) 107263.

[15] D. Ocepek, M. Kodrič, G. Čepon, M. Boltežar, On the estimation of structural admittances from acoustic measurement using a dynamic substructuring approach, Applied Acoustics 180 (2021) 108115.

[16] Y. Chen, P. Avitabile, J. Dodson, Data consistency assessment function (DCAF), Mechanical Systems and Signal Processing 141 (2020) 106688.

[17] Z. Saeed, C. M. Firrone, T. M. Berruti, Joint identification through hybrid models improved by correlations, Journal of Sound and Vibration 494 (2021) 115889.

[18] M. Kodrič, G. Čepon, M. Boltežar, Experimental framework for identifying inconsistent measurements in frequency-based substructuring, Mechanical Systems and Signal Processing 154 (2021) 107562.

[19] D. de Klerk, D. J. Rixen, J. de Jong, The frequency based substructuring (FBS) method reformulated according to the dual domain decomposition method, in: Proceedings of the 24th International Modal Analysis Conference, A Conference on Structural Dynamics, 2006, pp. 1–14.

[20] D. Klerk, D. Rixen, S. Voormeeren, General framework for dynamic substructuring: History, review, and classification of techniques, AIAA Journal 46 (2008) 1169–1181.

[21] M. S. Allen, R. L. Mayes, E. J. Bergman, Experimental modal substructuring to couple and uncouple substructures with flexible fixtures and multi-point connections, Journal of Sound and Vibration 329 (23) (2010) 4891–4906.

[22] R. W. Cottle, Manifestations of the schur complement, Linear Algebra and its Applications 8 (3) (1974) 189–211.

[23] R. J. Allemang, The modal assurance criterion–twenty years of use and abuse, Sound and vibration 37 (8) (2003) 14–23.

[24] M. van der Seijs, D. van den Bosch, D. J. Rixen, D. de Klerk, An improved methodology for the virtual point transformation of measured frequency response functions in dynamic substructuring, Proceedings of the 4th COMPDYN (2014).

[25] B. Peeters, H. Van der Auweraer, P. Guillaume, J. Leuridan, The PolyMAX frequency-domain method: a new standard for modal parameter estimation?, Shock and Vibration 11 (3, 4) (2004) 395–409.

[26] T. Bregar, A. El Mahmoudi, M. Kodrič, D. Ocepek, F. Trainotti, M. Pogačar, M. Göldeli, G. Čepon, M. Boltežar, D. J. Rixen, pyFBS: A python package for frequency based substructuring, Journal of Open Source Software 7 (69) (2022) 3399.

[27] F. Trainotti, T. Bregar, S. Klaassen, D. Rixen, Experimental decoupling of substructures by singular vector transformation, Mechanical Systems and Signal Processing 163 (2022) 108092.